

# Multiplierless DFT Approximation Based on the Prime Factor Algorithm

L. Portella\*

F. M. Bayer†

R. J. Cintra‡

## Abstract

Matrix approximation methods have successfully produced efficient, low-complexity approximate transforms for the discrete cosine transforms and the discrete Fourier transforms. For the DFT case, literature archives approximations operating at small power-of-two blocklengths, such as {8, 16, 32}, or at large blocklengths, such as 1024, which are obtained by means of the Cooley-Tukey-based approximation relying on the small-blocklength approximate transforms. Cooley-Tukey-based approximations inherit the intermediate multiplications by twiddled factors which are usually not approximated; otherwise the effected error propagation would prevent the overall good performance of the approximation. In this context, the prime factor algorithm can furnish the necessary framework for deriving fully multiplierless DFT approximations. We introduced an approximation method based on small prime-sized DFT approximations which entirely eliminates intermediate multiplication steps and prevents internal error propagation. To demonstrate the proposed method, we design a fully multiplierless 1023-point DFT approximation based on 3-, 11- and 31-point DFT approximations. The performance evaluation according to popular metrics showed that the proposed approximations not only presented a significantly lower arithmetic complexity but also resulted in smaller approximation error measurements when compared to competing methods.

## Keywords

Fast algorithms, approximate DFT, multiplicative complexity, prime factor algorithm.

## 1 Introduction

The discrete Fourier transform (DFT) is a central tool in signal processing [9], finding applications in a very large number of contexts, such as spectral analysis [74], filtering [64], data compression [69], and fast convolution [11], to cite a few. The widespread usage of the DFT is due to its rich physical interpretation [10] and the existence of efficient methods for its computation [61]. Although the direct computation of the  $N$ -point DFT is an operation in  $\mathcal{O}(N^2)$ —which is prohibitively expensive [35]—efficient algorithms [10, 15, 61] collectively known as fast Fourier transforms (FFTs) [6] are capable of evaluating the DFT with much less numerical operations placing the resulting complexity in  $\mathcal{O}(N \log N)$  [15].

Despite such substantial reduction in complexity, the remaining operations can still be significant in contexts where severe restrictions in computational power and/or energy autonomy are present [48]. Such restrictive conditions arise in the framework of wireless communication [54, 85], embedded systems [44, 49], and Internet of Things (IoT) [50, 73].

Inspired by the successful methods for approximating the discrete cosine transform [5, 7, 8, 12, 19, 21, 22, 33], in [75], a suite of multiplierless DFT approximations was derived for  $N = 8, 16$ , and  $32$  [2, 20, 46, 52, 53, 76]. These DFT approximations were demonstrated to provide spectral estimates close to the exact DFT computation, while requiring only 26, 54, and 144 additions for real-valued input, respectively [20, 75]. Broadly, finding approximate transforms that closely match the performance of the exact ones is a hard task, because it is often posed as an integer non-linear matrix optimization problem with a large number of variables [27]. Thus, as  $N$  increases, obtaining good approximations becomes an exceedingly demanding problem to be solved [65]. As a consequence, designers of DFT approximations make use of indirect methods such as (i) mathematical relationships between small-sized and large-sized DFT matrices [15], (ii) matrix functional recursions [62], and (iii) matrix decompositions [70]. The systematic derivation of good DFT approximations

\*L. Portella was with the Department of Statistics, Universidade Estadual de Campinas, Campinas 13083-859, Brazil and the Industrial Signal Processing Laboratory, Universidade Federal de Pernambuco, Caruaru, Brazil (e-mail: luangs@unicamp.br).

†F. M. Bayer is with the Department of Statistics and LACESM, Universidade Federal de Santa Maria, Santa Maria 97105-900, Brazil and the Department of Mathematics and Natural Sciences, Blekinge Institute of Technology, Karlskrona, 37179, Sweden (e-mail: bayer@ufsm.br).

‡R. J. Cintra is with the Industrial Signal Processing Laboratory, Department of Technology, Universidade Federal de Pernambuco, Caruaru 55014-900, Brazil (e-mail: rjpsc@de.ufpe.br).

for large block sizes is still an open problem and technical advances occur in a case-by-case fashion due to the inherent numerical difficulties of finding integer matrices that ensure competitive performance.

Following such an indirect approach, the 32-point DFT approximation discussed in [20, 75] was employed as the fundamental block of the 1024-point DFT approximation introduced in [53]. When employed as a fundamental block to obtain larger transforms, the DFT is referred to as a ground transformation. The methodology described in [53] revisits the Cooley-Tukey algorithm and effectively extends a given 32-point DFT approximation resulting in a  $32^2$ -point DFT approximation. This extension stems from the fact that the Cooley-Tukey algorithm can be formulated according to a two-dimensional mapping such that the computation of the 1024-point DFT is performed by  $2 \times 32$  instantiations of the 32-point DFT [25]. However, even considering multiplierless 32-point DFT approximations, the resulting 1024-point DFT approximations proposed in [53] are not multiplication-free. Indeed, the Cooley-Tukey-based approximations inherit the twiddle factors present in the exact formulation of the traditional Cooley-Tukey algorithm [61]. Thus, the final resulting arithmetic complexity of the best Cooley-Tukey-based 1024-point DFT approximation in [53] is 2883 real multiplications and 25155 additions, which represent approximately a 72% reduction in terms of real multiplication and an 18% reduction in terms of additions when compared to the exact Cooley-Tukey algorithm [6].

The goal of the present paper is to propose a framework for deriving large DFT approximations that are fully multiplierless. Although, in fixed-point arithmetic, any multiplication can theoretically be expressed as a sum of dyadic terms, we adopt the term multiplierless in a more restrictive and practical sense, consistent with [12], where the minimum number of adders is sought. In this work, matrices elements assumes values in  $\{0, \pm 1, \pm \frac{1}{2}\}$  and eventual scaling constants have their dyadic representation limited to at most two additions. Such multiplierlessness criterion emphasizes that the proposed approximations rely only on additions and bit-shifting operations, aiming at the minimum number of adders, so that future implementations can achieve reductions in chip area, power consumption, and delay [2]. For such an end, we aim at exploiting the prime factor algorithm (PFA) [31, 78], also known as the Good-Thomas algorithm. The PFA has distinct number-theoretical properties capable of performing the DFT computation without intermediate computations such as twiddle factors, which the traditional radix-2 algorithm heavily rely on. This approach allows the construction of scalable, multiplierless DFT approximations, significantly reducing arithmetic complexity while maintaining competitive approximation accuracy.

Due to the very number-theoretical nature of the PFA, the resulting transform blocklength cannot be a power-of-two [6]. However, the design of non-power-of-two DFT methods [57, 80, 84] is a promising topic in (i) beamforming and direction of arrival (DOA) estimation [1, 60, 68, 71, 79, 81]; (ii) 5G broadcasting which usually present  $2^n \cdot 3^m$ -point ( $n \leq 11$ ) input signals [24]; (iii) hybrid algorithms [42, 72]; (iv) when the length cannot be chosen, such as in digital radio technology [23, 39, 43, 47]; (v) channel equalization [13, 45]; and (vi) scenarios that presents flexible or adaptive transform lengths as LTE [17] and MIMO-OFDM systems [83]. For examples, FFT blocklengths like 128, 512, 1024, and 2048, which are usually implemented with radix-2 algorithms, could be replaced by alternative lengths such as 130 ( $2 \times 5 \times 13$ ), 510 ( $2 \times 3 \times 5 \times 17$ ), 1023 (which is adopted in this work to demonstrate the proposed method), and 2046 ( $2 \times 3 \times 11 \times 31$ ), which are compatible with the PFA. Although power-of-two DFT algorithms are more common, in the end, the total number of operations might play a decisive role.

As a consequence, we separated the particular blocklength  $N = 1023$  as a representative case study to highlight the benefits of the proposed approach in contrast with the state-of-the-art in large-scale DFT approximations introduced in [53]. The comparison justified by the fact that in [53] it is provided a practical implementation benchmark for low-power applications such as beamforming, reinforcing the relevance of a direct comparison. Other multiplierless strategies based on twiddle-factor approximations, such as those using sum-of-powers-of-two (SOPOT) coefficients [16] and streaming multiplierless FFTs (SMUL-FFT) [58], are also effective in specific contexts. However, these methods tend to be more suitable for small-to-medium transform sizes. As the blocklength increases, the number of distinct twiddle-factor matrices to be approximated grows rapidly, shifting the computational burden from multiplications to managing a large number of additive operations or fixed-pattern multipliers. This can significantly reduce their practical efficiency in large-scale settings.

It is worth emphasizing that, although this work focuses on the 1023-point DFT approximation to enable a direct comparison with the method in [53], the proposed approach is built upon the PFA, which naturally inherits scalability to any blocklength that can be factorized into coprime factors. This scalability stems from the Chinese Remainder Theorem, which underlies the Good–Thomas mapping and enables the decomposition of large transforms into smaller ground transforms. Furthermore, it is also possible to develop hybrid algorithms where radix-2 process the power-of-two factors, while the proposed PFA-based multiplierless method computes the remaining coprime factors.

The paper is organized as follows. Section 2 provides an overview of the DFT and the PFA. Section 3 describes the methodology to obtain the proposed DFT approximation. In Section 4, the proposed approximations and algorithm are detailed. In Section 5, the proposed method is employed to propose a multiplierless 1023-point DFT approximation. Fast algorithms and arithmetic complexity are presented in Section 6. Section 7 reports the error analysis of the approximations. In Section 8, conclusions are summarized.

## 2 Mathematical background

In this section, we review the DFT mathematical background and briefly describe the prime factor algorithm.

### 2.1 Definition of the DFT

The DFT is a linear transformation that maps an  $N$ -point discrete signal  $\mathbf{x} = [x[0], x[1], \dots, x[N-1]]^\top$  into an output signal  $\mathbf{X} = [X[0], X[1], \dots, X[N-1]]^\top$  by means of the following expression [6]:

$$X[k] \triangleq \sum_{n=0}^{N-1} \omega_N^{nk} \cdot x[n], \quad k = 0, 1, \dots, N-1, \quad (1)$$

where  $X[k]$  is the  $k$ th DFT coefficient,  $\omega_N = e^{-j\frac{2\pi}{N}}$  is the  $N$ th root of unity, and  $j \triangleq \sqrt{-1}$ . Although, the input signal  $\mathbf{x}$  may be real or complex, this work focuses on the general case of complex-valued inputs.

The DFT can also be expressed in matrix format according to the next expression:

$$\mathbf{X} = \mathbf{F}_N \cdot \mathbf{x},$$

where  $\mathbf{F}_N$  is the DFT matrix defined by

$$\mathbf{F}_N = \begin{bmatrix} 1 & 1 & 1 & \dots & 1 \\ 1 & \omega_N & \omega_N^2 & \dots & \omega_N^{N-1} \\ 1 & \omega_N^2 & \omega_N^4 & \dots & \omega_N^{2(N-1)} \\ 1 & \omega_N^3 & \omega_N^6 & \dots & \omega_N^{3(N-1)} \\ \vdots & \vdots & \vdots & \ddots & \vdots \\ 1 & \omega_N^{N-1} & \omega_N^{2(N-1)} & \dots & \omega_N^{(N-1)(N-1)} \end{bmatrix}.$$

### 2.2 Prime Factor Algorithm

Comparable to the more popular Cooley-Tukey FFT [6], the PFA is a factorization-based FFT capable of computing the  $N$ -point DFT, where  $N = N_1 \times N_2$ , with  $N_1$  and  $N_2$  being relatively prime, i.e.,  $\gcd(N_1, N_2) = 1$ . The method is based on a number-theoretical re-indexing [61] of the input signal coefficients into a two-dimensional array [64] which is based on the Chinese remainder theorem [6].

The PFA is summarized according to the following description [6, Fig. 3.8]:

- Obtain  $n_1$  and  $n_2$  that satisfy  $(n_1 \cdot N_1 + n_2 \cdot N_2) \bmod N = 1$  [61];

(ii) Map  $\mathbf{x}$  into a block of size  $N_1 \times N_2$  according to the following 1D to 2D rearrangement of elements:

$$\text{map} \left( \begin{bmatrix} x[0] \\ x[1] \\ x[2] \\ \vdots \\ x[N-1] \end{bmatrix} \right) = \begin{bmatrix} x[0] & x[r] & \dots & x[(N_2-1)r] \\ x[s] & x[r+s] & \dots & x[r+(N_2-1)r] \\ \vdots & \vdots & \ddots & \vdots \\ x[(N_1-1)s] & x[(N_1-1)r+s] & \dots & x[(N_1-1)s+(N_2-1)r] \end{bmatrix},$$

where  $r = N_1 \cdot n_1$  and  $s = N_2 \cdot n_2$ ;

(iii) Compute the  $N_2$ -point DFT of each column of the 2D array obtained in Step 2);

(iv) Compute the  $N_1$ -point DFT of each row of the resulting 2D array from Step 3);

(v) Reconstruct the vector  $\mathbf{X}$  from the resulting block according to the following mapping:

$$\text{invmap} \left( \begin{bmatrix} X[0] & X[N_1] & \dots & X[(N_2-1)N_1] \\ X[N_2] & X[N_1+N_2] & \dots & X[N_2+(N_2-1)N_1] \\ \vdots & \vdots & \ddots & \vdots \\ X[(N_1-1)N_2] & X[(N_1-1)N_2+N_1] & \dots & X[(N_1-1)N_2+(N_2-1)N_1] \end{bmatrix} \right) = \begin{bmatrix} X[0] \\ X[1] \\ X[2] \\ \vdots \\ X[N-1] \end{bmatrix}.$$

All index operations are performed in modulo  $N$  arithmetic, ensuring the correct size of the arrays. The algorithm can be synthesized as follows:

$$\mathbf{X} = \text{invmap} \left( \mathbf{F}_{N_1} \cdot \left[ \mathbf{F}_{N_2} \cdot (\text{map}(\mathbf{x}))^\top \right]^\top \right). \quad (2)$$

Notice that if  $N_1$  or  $N_2$  can be factored into relative primes, then the algorithm can be reapplied. The  $N_1$ - and  $N_2$ -point transformations are referred to as ground transformations.

### 3 Approximate DFT methodology

Being alternatives to the exact transformations, approximate transforms possess a low computational cost and provide similar mathematical properties and performance to their exact counterparts. In this context, an approximate DFT matrix  $\hat{\mathbf{F}}_N^*$  can be derived by solving the following optimization problem:

$$\hat{\mathbf{F}}_N^* = \arg \min_{\hat{\mathbf{F}}_N} \text{error}(\hat{\mathbf{F}}_N, \mathbf{F}_N), \quad (3)$$

where  $\text{error}(\cdot)$  represents the adopted error measure and  $\hat{\mathbf{F}}_N$  is a candidate approximation obtained from a suitable search space.

Approximate transforms can be derived from low-complexity matrices [19] according to an orthogonalization process referred to as polar decomposition [37]. Such approach consists of two matrices: a low-complexity matrix and a real-valued diagonal matrix. It is important to note that an auxiliary method is required to generate the low-complexity matrix because the polar decomposition alone does not provide such a matrix. If the polar decomposition is applied directly to the exact DFT matrix or to an already orthogonal approximation, the resulting diagonal matrix becomes the identity matrix. The auxiliary method to obtain the low-complexity matrix is presented in the next section.

A candidate approximation  $\hat{\mathbf{F}}_N$  for the exact transformation  $\mathbf{F}_N$  can be written as:

$$\hat{\mathbf{F}}_N = \sqrt{N} \cdot \mathbf{S}_N \cdot \mathbf{T}_N, \quad (4)$$

where  $\mathbf{T}_N$  is a low-complexity matrix and  $\mathbf{S}_N$  is a diagonal matrix expressed by

$$\mathbf{S}_N = \text{diag}\left(\sqrt{\left[\text{diag}\left(\mathbf{T}_N \cdot \mathbf{T}_N^H\right)\right]^{-1}}\right), \quad (5)$$

being  $\text{diag}(\cdot)$  a function that returns a diagonal matrix, if the argument is a vector; or a vector with the diagonal elements, if the argument is a matrix, the superscript  $H$  denotes the Hermitian operation [70], and  $\sqrt{\cdot}$  is the matrix square root operation [38]. Therefore, a suitable choice of  $\mathbf{T}_N$  is central to the above approach. Thus, from this point onward, we focus on the derivation of  $\mathbf{T}_N$ . For simplicity of notation, the constant  $\sqrt{N}$  is absorbed into the matrix  $\mathbf{S}_N$  as follows

$$\hat{\mathbf{F}}_N = \hat{\mathbf{S}}_N \cdot \mathbf{T}_N, \quad (6)$$

where  $\hat{\mathbf{S}}_N = \sqrt{N} \cdot \mathbf{S}_N$ .

### 3.1 Search Space

The low-complexity matrices  $\mathbf{T}_N$  are taken from the search space given by the matrix space  $\mathcal{M}_N(\mathcal{P})$ , which is the set of all  $N \times N$  matrices with entries over a set of low-complexity multipliers  $\mathcal{P}$ . Popular choices for  $\mathcal{P}$  are  $\{-1, 0, 1\}$  and  $\{-1, -\frac{1}{2}, 0, \frac{1}{2}, 1\}$ , which contain only trivial multipliers [6].

The set  $\mathcal{M}_N(\mathcal{P})$  can be extremely large. For instance,  $\mathcal{M}_N(\mathcal{P})$  contains  $3^{64} \approx 3.43 \times 10^{30}$  elements (distinct matrices) for  $N = 8$  and  $\mathcal{P} = \{-1, 0, 1\}$ . Therefore, we propose as a working search space, a subset of  $\mathcal{M}_N(\mathcal{P})$  given by the expansion factor methodology [12]. Thus, low-complexity matrices  $\mathbf{T}_N$  can be generated according to the following expression:

$$\mathbf{T}_N = g(\alpha \cdot \mathbf{F}_N), \quad (7)$$

where  $g(\cdot)$  is an entry-wise integer matrix function, such as rounding, truncation, ceiling, and floor functions [19] and  $\alpha$  is a real number referred to as the expansion factor [55]. To ensure that the integer function  $g(\cdot)$  returns only values within  $\mathcal{P}$ , the values of  $\alpha$  are judiciously restricted to an interval  $\mathcal{D}$  given by

$$\alpha_{\min} \leq \alpha \leq \alpha_{\max}, \quad (8)$$

where  $\alpha_{\min} = \inf\{\alpha \in \mathbb{R}_+ : g(\alpha \cdot \gamma_{\max}) \neq 0\}$  and  $\alpha_{\max} = \sup\{\alpha \in \mathbb{R}_+ : g(\alpha \cdot \gamma_{\max}) = \max(\mathcal{P})\}$ , being  $\gamma_{\max} = \max_{m,n}(|\Re(f_{m,n})|, |\Im(f_{m,n})|)$  and  $f_{m,n}$ , the  $(m,n)$ th entry of  $\mathbf{F}_N$ . The symmetries of  $\mathbf{F}_N$  allow us to restrict the analysis to  $\alpha \geq 0$  and since the entries of  $\mathbf{F}_N$  are bounded by the unity,  $\gamma_{\max} = 1$ .

### 3.2 Optimization Problem and Objective Function

The general optimization problem shown in (3) can be formulated as

$$\alpha^* = \underset{\alpha \in \mathcal{D}}{\text{argmin}} \text{error}(\hat{\mathbf{F}}_N, \mathbf{F}_N), \quad (9)$$

employing (6)

$$\alpha^* = \underset{\alpha \in \mathcal{D}}{\text{argmin}} \text{error}(\hat{\mathbf{S}}_N \cdot \mathbf{T}_N, \mathbf{F}_N), \quad (10)$$

and rewritten applying (7)

$$\alpha^* = \underset{\alpha \in \mathcal{D}}{\arg \min} \text{error}(\hat{\mathbf{S}}_N \cdot g(\alpha \cdot \mathbf{F}_N), \mathbf{F}_N). \quad (11)$$

Therefore, the low-complexity matrix is obtained by

$$\mathbf{T}_N^* = g(\alpha^* \cdot \mathbf{F}_N), \quad (12)$$

and the optimal approximation is furnished by

$$\hat{\mathbf{F}}_N^* = \hat{\mathbf{S}}_N^* \cdot \mathbf{T}_N^*, \quad (13)$$

where  $\hat{\mathbf{S}}_N^*$  stems from  $\mathbf{T}_N^*$  as detailed in (5), *mutatis mutandis*.

Now we aim at specifying the error function in (11). As shown in literature [52, 66, 77], usual choices for such function are: (i) the total error energy [21]; (ii) the mean absolute percentage error (MAPE) [28]; and (iii) the deviation from orthogonality [22, 29]. These metrics are described below.

(i) The total error energy is defined by

$$\epsilon(\hat{\mathbf{F}}_N) = \pi \cdot \|\mathbf{F}_N - \hat{\mathbf{F}}_N\|_F^2,$$

where  $\|\cdot\|_F$  represents the Frobenius norm [82];

(ii) The MAPE of the transformation matrix is obtained by

$$M(\hat{\mathbf{F}}_N) = 100 \cdot \frac{1}{N^2} \cdot \sum_{m=1}^N \sum_{n=1}^N \left| \frac{f_{m,n} - \hat{f}_{m,n}}{f_{m,n}} \right|,$$

where  $\hat{f}_{m,n}$  is the  $(m, n)$ th entry of  $\hat{\mathbf{F}}_N$ ;

(iii) The deviation from orthogonality [22] is defined by:

$$\phi(\hat{\mathbf{F}}_N) = 1 - \frac{\|\text{diag}(\hat{\mathbf{F}}_N \cdot \hat{\mathbf{F}}_N^H)\|_F}{\|\hat{\mathbf{F}}_N \cdot \hat{\mathbf{F}}_N^H\|_F}.$$

Small values of  $\phi(\cdot)$  indicate proximity to orthogonality. Orthogonal matrices have null deviation.

Combining the above error functions in a single optimization problem, we obtain the following multicriteria problem [4, 27]:

$$\alpha^* = \underset{\alpha \in \mathcal{D}}{\arg \min} \{ \epsilon(\hat{\mathbf{S}}_N^* \cdot g(\alpha \cdot \mathbf{F}_N)), M(\hat{\mathbf{S}}_N^* \cdot g(\alpha \cdot \mathbf{F}_N)), \phi(\hat{\mathbf{S}}_N^* \cdot g(\alpha \cdot \mathbf{F}_N)) \}. \quad (14)$$

## 4 Multiplierless Prime Factor Approximation

In this section, we formalize the mathematical structure of the approximate DFT based on the prime factor algorithm. Additional to the main structure, we describe two variations of the method: (i) the unscaled approximation and (ii) the hybrid approximation.

## 4.1 Mathematical Definition

Under the assumption of the PFA, we compute the  $N$ -point DFT approximation as follows

$$\hat{\mathbf{X}} = \text{invmap} \left( \hat{\mathbf{F}}_{N_1}^* \cdot \left[ \hat{\mathbf{F}}_{N_2}^* \cdot (\text{map}(\mathbf{x}))^\top \right]^\top \right), \quad (15)$$

where  $\hat{\mathbf{F}}_{N_1}^*$  and  $\hat{\mathbf{F}}_{N_2}^*$  are approximations of  $\mathbf{F}_{N_1}$  and  $\mathbf{F}_{N_2}$ , respectively (cf. (2)).

If the approximations used in (15) admit the format expressed in (13), then the above equation can be rewritten as

$$\hat{\mathbf{X}} = \text{invmap} \left( \hat{\mathbf{S}}_{N_1}^* \cdot \mathbf{T}_{N_1}^* \cdot \left[ \hat{\mathbf{S}}_{N_2}^* \cdot \mathbf{T}_{N_2}^* \cdot (\text{map}(\mathbf{x}))^\top \right]^\top \right). \quad (16)$$

Notice that  $\hat{\mathbf{S}}_{N_1}^*$  and  $\hat{\mathbf{S}}_{N_2}^*$  are real diagonal matrices that can be factored out from the mapping operator as follows:

$$\hat{\mathbf{X}} = \hat{\mathbf{S}} \cdot \text{invmap} \left( \mathbf{T}_{N_1}^* \cdot \left[ \mathbf{T}_{N_2}^* \cdot (\text{map}(\mathbf{x}))^\top \right]^\top \right), \quad (17)$$

where  $\hat{\mathbf{S}}$  is a diagonal matrix given by  $\hat{\mathbf{S}} = \text{diag} \left[ \text{invmap} \left( \text{diag}(\hat{\mathbf{S}}_{N_1}^*) \cdot \text{diag}(\hat{\mathbf{S}}_{N_2}^*)^\top \right) \right]$ .

## 4.2 Unscaled Approximation

Because the matrix  $\hat{\mathbf{S}}$  is diagonal, its role in the approximate DFT computation consists of scaling each spectral component. Depending on the context in which the DFT is applied, the scaling can be embedded, absorbed, parallel computed, or even neglected when the unscaled spectrum is sufficient [30, 41, 67]. The unscaled  $N$ -point DFT approximation is obtained by

$$\tilde{\mathbf{X}} = \text{invmap} \left( \mathbf{T}_{N_1}^* \cdot \left[ \mathbf{T}_{N_2}^* \cdot (\text{map}(\mathbf{x}))^\top \right]^\top \right). \quad (18)$$

Thus, we have the following relationship between (17) and (18):

$$\hat{\mathbf{X}} = \hat{\mathbf{S}} \cdot \tilde{\mathbf{X}}. \quad (19)$$

## 4.3 Hybrid Approximations

It might be advantageous to approximate only part of the DFT computation instead of the entire transform. This approach called hybrid algorithms allows for a balance between computational efficiency and accuracy, targeting specific components of the computation for approximation. In this context, we also provide two hybrid algorithms approximating only part of the DFT computation.

First, we keep the row-wise  $N_1$ -point DFT exact while the column-wise  $N_2$ -point DFT is approximated. The diagonal matrix  $\hat{\mathbf{S}}$  can also be factored out in the hybrid algorithms. Thus, this algorithm is given by

$$\hat{\mathbf{X}}_1 = \hat{\mathbf{S}} \cdot \text{invmap} \left( \left\{ \mathbf{F}_{N_1} \cdot \left[ \mathbf{T}_{N_2}^* \cdot (\text{map}(\mathbf{x}))^\top \right]^\top \right\}^\top \right), \quad (20)$$

where  $\hat{\mathbf{S}} = \text{diag} \left[ \text{invmap} \left( \mathbf{1}_{N_1} \cdot \text{diag}(\hat{\mathbf{S}}_{N_2}^*)^\top \right) \right]$  and  $\mathbf{1}_r$  is a column vector of ones with length equals to  $r$ .

Second, the column-wise  $N_2$ -point DFT is maintained exact and the row-wise  $N_1$ -point DFT is approximated. Then, the  $N$ -point DFT approximation is calculated by

$$\hat{\mathbf{X}}_2 = \hat{\mathbf{S}} \cdot \text{invmap} \left( \left\{ \mathbf{T}_{N_1}^* \cdot \left[ \mathbf{F}_{N_2} \cdot (\text{map}(\mathbf{x}))^\top \right]^\top \right\}^\top \right), \quad (21)$$

where  $\hat{\mathbf{S}} = \text{diag} \left[ \text{invmap} \left( \text{diag}(\hat{\mathbf{S}}_{N_1}^*) \cdot (\mathbf{1}_{N_2})^\top \right) \right]$ .

## 5 Approximations for the 1023-point DFT

In this section, we advance two results. First, we apply the prime factor algorithm detailed in Section 4 to obtain approximations for the 1023-point DFT. Second, we apply the methodology described in Section 3 to obtain approximations for the 3-, 11- and, 31-point DFTs, which are required for 1023-point DFT approximations.

### 5.1 1023-point DFT Approximation

Invoking (15) for  $N_1 = 31$  and  $N_2 = 33$ , we introduce a 1023-point DFT approximation according to the following equation:

$$\hat{\mathbf{X}} = \text{invmap} \left( \hat{\mathbf{F}}_{31}^* \cdot \left[ \hat{\mathbf{F}}_{33}^* \cdot (\text{map}(\mathbf{x}))^\top \right]^\top \right). \quad (22)$$

The term in square brackets in (22) requires 31 calls of a 33-point DFT approximation. Because  $N_2 = 33 = 11 \times 3$  is suitable for the proposed method formalism, a 33-point DFT approximation can be obtained based on approximations for the 3- and 11-point DFTs, as follows

$$\hat{\mathbf{Y}} = \text{invmap} \left( \hat{\mathbf{F}}_{11}^* \cdot \left[ \hat{\mathbf{F}}_3^* \cdot (\text{map}(\mathbf{y}))^\top \right]^\top \right), \quad (23)$$

where  $\mathbf{y}$  is the 33-point column vector corresponding to the rows of  $\text{map}(\mathbf{x})$ . As shown in (17), the scaling matrix  $\hat{\mathbf{S}}$  can be calculated separately, allowing the 1023-point DFT approximation to be rewritten as

$$\hat{\mathbf{X}} = \hat{\mathbf{S}} \cdot \text{invmap} \left( \hat{\mathbf{T}}_{31}^* \cdot \left[ \hat{\mathbf{T}}_{33}^* \cdot (\text{map}(\mathbf{x}))^\top \right]^\top \right), \quad (24)$$

and

$$\hat{\mathbf{Y}} = \text{invmap} \left( \hat{\mathbf{T}}_{11}^* \cdot \left[ \hat{\mathbf{T}}_3^* \cdot (\text{map}(\mathbf{y}))^\top \right]^\top \right). \quad (25)$$

Notice that the diagonal matrix  $\hat{\mathbf{S}}$  encompasses the intermediate diagonals  $\hat{\mathbf{S}}_3^*$ ,  $\hat{\mathbf{S}}_{11}^*$ , and  $\hat{\mathbf{S}}_{31}^*$  and is given by

$$\hat{\mathbf{S}} = \text{diag} \left\{ \text{invmap} \left[ \text{diag}(\hat{\mathbf{S}}_{31}^*) \cdot \text{invmap} \left( \text{diag}(\hat{\mathbf{S}}_{11}^*) \cdot \text{diag}(\hat{\mathbf{S}}_3^*)^\top \right)^\top \right] \right\},$$

where  $\hat{\mathbf{S}}_3^*$ ,  $\hat{\mathbf{S}}_{11}^*$ , and  $\hat{\mathbf{S}}_{31}^*$  are the diagonal matrices required by the DFT approximations  $\hat{\mathbf{F}}_3^*$ ,  $\hat{\mathbf{F}}_{11}^*$ , and  $\hat{\mathbf{F}}_{31}^*$ , respectively, as described in (13).

### 5.2 Design Parameters

The algorithm detailed in the previous section requires approximations to the 3-, 11-, and 31-point DFT. To obtain such approximations, we numerically apply the methodology described in Section 3 for which  $g(\cdot)$  and  $\mathcal{P}$  must be specified. As suggested in [77], we define  $\mathcal{P} = \{-1, -\frac{1}{2}, 0, \frac{1}{2}, 1\}$  as the set of low-complexity multipliers. Among the integer functions mentioned, the round function, as implemented in Matlab/Octave [26, 56], has been reported to offer superior performance when compared with other integer functions [21, 22, 77]. Thus, as suggested in [63], we adopted the following round-to-multiple function:

$$g(x) = \frac{1}{2} \cdot \text{round}(2 \cdot x) \in \mathcal{P}. \quad (26)$$

The related  $\alpha$  search space is  $\mathcal{D} = [0.26, 1.25]$  (cf. (8)). The  $\alpha$  step used was  $10^{-5}$  providing a total of 6, 16, and 42 different approximations for the 3-, 11-, and 31-point DFTs, respectively. Smaller  $\alpha$  steps do not alter the results.

### 5.3 3-, 11-, and 31-point DFT Approximations

The obtained optimal expansion factors  $\alpha^*$  are in the intervals  $[0.86603, 1.25000]$ ,  $[0.99240, 1.14528]$ , and  $[1.08859, 1.15141]$  for the 3-, 11-, and 31-point DFT approximations, respectively. Therefore, we selected  $\alpha^* = \frac{9}{8}$  for convenience. Then, the low-complexity matrices  $\mathbf{T}_3^*$ ,  $\mathbf{T}_{11}^*$ , and  $\mathbf{T}_{31}^*$  are obtained by

$$\mathbf{T}_N^* = \frac{1}{2} \cdot \text{round} \left( 2 \cdot \frac{9}{8} \cdot \mathbf{F}_N \right), \quad N = 3, 11, 31.$$

From (5), we obtain the scaling matrices  $\hat{\mathbf{S}}_N^*$  according to the following general structure

$$\hat{\mathbf{S}}_N^* = \text{diag} \left( 1, \sqrt{\eta_N} \cdot \mathbf{I}_{N-1} \right), \quad N = 3, 11, 31,$$

where  $\mathbf{I}_m$  is the identity matrix of order  $m$ , and the constants are  $\eta_3 = \frac{6}{7}$ ,  $\eta_{11} = \frac{11}{13}$ , and  $\eta_{31} = \frac{31}{38}$ .

Thus, the 3-, 11- and 31-point DFT approximations are obtained by

$$\hat{\mathbf{F}}_N^* = \hat{\mathbf{S}}_N^* \cdot \mathbf{T}_N^*, \quad N = 3, 11, 31.$$

### 5.4 Approximate Scale Factors

Despite the dramatic reduction in arithmetic complexity, including the absence of twiddle factors, the computation shown in (24) requires  $2(N - 1)$  real multiplications due to the elements of the diagonal  $\hat{\mathbf{S}}$ . The elements of  $\hat{\mathbf{S}}$ ,  $s_i, i = 0, 1, \dots, 1022$ , are given by

$$s_i = \begin{cases} 1, & \text{if } i = 0, \\ \sqrt{\frac{6}{7}}, & \text{if } i \bmod 31 = 0 \wedge i \bmod 11 = 0 \wedge i \bmod 3 \neq 0, \\ \sqrt{\frac{11}{13}}, & \text{if } i \bmod 31 = 0 \wedge i \bmod 11 \neq 0 \wedge i \bmod 3 = 0, \\ \sqrt{\frac{66}{91}}, & \text{if } i \bmod 31 = 0 \wedge i \bmod 11 \neq 0 \wedge i \bmod 3 \neq 0, \\ \sqrt{\frac{31}{38}}, & \text{if } i \bmod 31 \neq 0 \wedge i \bmod 11 = 0 \wedge i \bmod 3 = 0, \\ \sqrt{\frac{93}{133}}, & \text{if } i \bmod 31 \neq 0 \wedge i \bmod 11 = 0 \wedge i \bmod 3 \neq 0, \\ \sqrt{\frac{341}{494}}, & \text{if } i \bmod 31 \neq 0 \wedge i \bmod 11 \neq 0 \wedge i \bmod 3 = 0, \\ \sqrt{\frac{1023}{1729}}, & \text{otherwise.} \end{cases}$$

Further complexity reductions can be achieved by approximating the elements of  $\hat{\mathbf{S}}$  using truncated representations from the canonical signed digit (CSD) number system [18, 36], which satisfy the minimum adder representation criterion [32]. We approximated each element in  $\hat{\mathbf{S}}$  in such way that its truncated CSD representation admits at most two additions [3]. Table 1 provides a representation of the elements from  $\hat{\mathbf{S}}$ , the absolute error between the approximation, the constants, and their truncated representation in CSD ( $\bar{1}$  represents  $-1$ ). Since the elements from  $\hat{\mathbf{S}}_3$ ,  $\hat{\mathbf{S}}_{11}$ , and  $\hat{\mathbf{S}}_{31}$  are present in  $\hat{\mathbf{S}}$ , multiplierless approximation for the 3-, 11-, and 31-point DFTs are also possible using Table 1. The approximations in which the diagonal matrices were also approximated follow the notation  $\hat{\mathbf{F}}_N'$ .

## 6 Fast Algorithms and Arithmetic Complexity

In this section, we introduce fast algorithms based on sparse matrix factorizations [6] for the proposed 3-, 11-, and 31-point DFT approximations to reduce the number of remaining operations. These approximations are employed within the PFA to approximately compute the 1023-point DFT. Although the PFA has the inherent property of reducing the total number of operations by nearly half when the input is real-valued, as shown in [34], for the sake of generality and consistency, the analyses presented in this section are based on complex-valued input. A complex multiplication can be translated into

Table 1: Truncated CSD Approximations for the Constants from  $\mathbf{S}$

Constant	Approximation	Error	CSD
$\sqrt{\frac{66}{91}} \approx 0.85163$	$\frac{55}{64} = 0.859375$	0.00774	1.0010010
$\sqrt{\frac{11}{13}} \approx 0.91987$	$\frac{59}{64} = 0.921875$	0.00201	1.0001010
$\sqrt{\frac{6}{7}} \approx 0.92582$	$\frac{119}{128} = 0.9296875$	0.00387	1.0001001
$\sqrt{\frac{341}{494}} \approx 0.83083$	$\frac{27}{32} = 0.84375$	0.01292	1.0010100
$\sqrt{\frac{93}{133}} \approx 0.83621$	$\frac{27}{32} = 0.84375$	0.00754	1.0010100
$\sqrt{\frac{31}{38}} \approx 0.90321$	$\frac{29}{32} = 0.90625$	0.00304	1.0010100
$\sqrt{\frac{1023}{1729}} \approx 0.76920$	$\frac{49}{64} = 0.765625$	0.00358	1.0100010

three real multiplications and three real additions [6, p. 3]. The matrices  $\mathbf{T}_N^*$ ,  $N = 3, 11, 31$ , employed in the 1023-point DFT approximations do not require multiplications; only additions and bit-shifting operations are needed [12, p. 221].

In the following, the butterfly-structure matrix is defined as follows

$$\mathbf{B}_m = \begin{bmatrix} \mathbf{I}_{m/2} & \bar{\mathbf{I}}_{m/2} \\ -\bar{\mathbf{I}}_{m/2} & \mathbf{I}_{m/2} \end{bmatrix},$$

where  $m$  is an even integer and  $\bar{\mathbf{I}}_{m/2}$  is the counter-identity matrix [40] of order  $m/2$ .

## 6.1 3-point Approximation Fast algorithm

The low-complexity matrix  $\mathbf{T}_3^*$  can be represented as:

$$\mathbf{T}_3^* = \mathbf{A}_1^\top \cdot \mathbf{C}_1 \cdot \mathbf{A}_1, \quad (27)$$

where

$$\mathbf{A}_1 = \text{diag}(1, \mathbf{B}_2), \quad (28)$$

and the matrix  $\mathbf{C}_1$  is

$$\mathbf{C}_1 = \begin{bmatrix} 1 & 1 \\ 1 & -\frac{1}{2} \\ & -j \end{bmatrix}.$$

The matrix  $\mathbf{A}_1$  requires only 4 real additions and  $\mathbf{C}_1$  needs 4 real additions and 2 bit-shifting operations.

Considering a complex input, the direct implementation of the  $\mathbf{T}_3^*$  requires 20 additions and 8 bit-shifting operations. However, if the factorization in (27) is applied, then  $\mathbf{T}_3^*$  requires 12 real additions and 2 bit-shifting operations. To scale the approximation maintaining the exact  $\hat{\mathbf{S}}_3^*$ , 4 real multiplications are added to the previous arithmetic cost. This approximation is denoted by  $\hat{\mathbf{F}}_3^*$ . Otherwise, if the diagonal matrix is approximated, 8 additions and 8 bit-shifting operations are needed instead of the multiplications. This approximation is called  $\hat{\mathbf{F}}_3'$ .

## 6.2 11-point Approximation Fast Algorithm

For the 11-point approximation, the low-complexity matrix  $\mathbf{T}_{11}^*$  is given by

$$\mathbf{T}_{11}^* = \mathbf{A}_2^\top \cdot \mathbf{C}_2 \cdot \mathbf{A}_2, \quad (29)$$

where

$$\mathbf{A}_2 = \text{diag}(1, \mathbf{B}_{10}), \quad (30)$$

and the block matrix  $\mathbf{C}_2$  is

$$\mathbf{C}_2 = \text{diag} \left( \begin{bmatrix} 1 & 1 & 1 & 1 & 1 & 1 & 1 & 1 & 1 & 1 & 1 & 1 & 1 & 1 & 1 \\ 1 & 1 & 1 & \frac{1}{2} & \frac{1}{2} & -\frac{1}{2} & -\frac{1}{2} & -1 & -1 & -1 & -1 & -1 & -1 & -1 & -1 \\ 1 & 1 & \frac{1}{2} & -\frac{1}{2} & -1 & 1 & 1 & -\frac{1}{2} & -\frac{1}{2} & -\frac{1}{2} & -1 & -1 & -1 & -1 & -1 \\ 1 & -1 & \frac{1}{2} & 1 & 1 & -\frac{1}{2} & -1 & -\frac{1}{2} & -\frac{1}{2} & -\frac{1}{2} & -1 & -1 & -1 & -1 & -1 \\ 1 & -\frac{1}{2} & 1 & -1 & \frac{1}{2} & 1 & -\frac{1}{2} & -1 & -\frac{1}{2} & -\frac{1}{2} & -1 & -1 & -1 & -1 & -1 \\ 1 & -1 & 1 & -\frac{1}{2} & \frac{1}{2} & 1 & -\frac{1}{2} & -1 & -\frac{1}{2} & -\frac{1}{2} & -1 & -1 & -1 & -1 & -1 \end{bmatrix}, \begin{bmatrix} -j & j & -j & \frac{j}{2} & -\frac{j}{2} \\ j & -\frac{j}{2} & -\frac{j}{2} & j & -j \\ -j & -\frac{j}{2} & j & \frac{j}{2} & -j \\ \frac{j}{2} & j & \frac{j}{2} & -j & -j \\ -\frac{j}{2} & -j & -j & -j & -\frac{j}{2} \end{bmatrix} \right).$$

Matrix  $\mathbf{A}_2$  requires 20 real additions and  $\mathbf{C}_2$  needs 90 real additions and 40 bit-shifting operations.

While the direct implementation of the  $\mathbf{T}_{31}^*$  requires 380 additions and 160 bit-shifting operations, the factorization presented in (29) needs 130 real additions and 40 bit-shifting operations. The scaling to  $\mathbf{F}_{11}^*$  requires 20 extra multiplications. In terms of  $\mathbf{F}'_{11}$ , it needs 40 additions and 40 bit-shifting operations instead of 20 multiplications of  $\mathbf{F}_{11}^*$ .

### 6.3 31-point Approximation Fast Algorithm

The low-complexity matrix  $\mathbf{T}_{31}^*$  can be expressed as:

$$\mathbf{T}_{31}^* = \mathbf{A}_3^\top \cdot \mathbf{C}_3 \cdot \mathbf{A}_3, \quad (31)$$

where

$$\mathbf{A}_3 = \text{diag}(1, \mathbf{B}_{30}).$$

The matrix  $\mathbf{C}_3$  is a block matrix given by

$$\mathbf{C}_3 = \text{diag}(\mathbf{E}_1, \mathbf{E}_2),$$

where

$$\mathbf{E}_1 = \begin{bmatrix} 1 & 1 & 1 & 1 & 1 & 1 & 1 & 1 & 1 & 1 & 1 & 1 & 1 & 1 & 1 & 1 & 1 \\ 1 & 1 & 1 & 1 & 1 & \frac{1}{2} & \frac{1}{2} & -\frac{1}{2} & -\frac{1}{2} & -\frac{1}{2} & -1 & -1 & -1 & -1 & -1 & -1 & -1 \\ 1 & 1 & 1 & \frac{1}{2} & -\frac{1}{2} & -1 & -1 & -1 & -1 & -1 & -\frac{1}{2} & -\frac{1}{2} & \frac{1}{2} & 1 & 1 & 1 & 1 \\ 1 & 1 & \frac{1}{2} & -\frac{1}{2} & -1 & -1 & -1 & -\frac{1}{2} & 1 & 1 & 1 & \frac{1}{2} & -\frac{1}{2} & -1 & -1 & -1 & -1 & -1 \\ 1 & 1 & -1 & -1 & -\frac{1}{2} & 1 & 1 & \frac{1}{2} & -\frac{1}{2} & -1 & -1 & -\frac{1}{2} & \frac{1}{2} & 1 & 1 & 1 & 1 & 1 \\ 1 & 1 & -1 & -1 & -\frac{1}{2} & \frac{1}{2} & 1 & -1 & -\frac{1}{2} & -1 & -1 & -\frac{1}{2} & -\frac{1}{2} & 1 & 1 & 1 & 1 & 1 \\ 1 & \frac{1}{2} & -\frac{1}{2} & -1 & -\frac{1}{2} & \frac{1}{2} & 1 & 1 & -\frac{1}{2} & -1 & -1 & -\frac{1}{2} & -\frac{1}{2} & 1 & 1 & 1 & 1 & 1 \\ 1 & \frac{1}{2} & -1 & -1 & 1 & \frac{1}{2} & -\frac{1}{2} & -1 & 1 & 1 & -\frac{1}{2} & -\frac{1}{2} & 1 & 1 & -1 & -1 & -1 & -1 \\ 1 & \frac{1}{2} & -1 & -1 & 1 & -\frac{1}{2} & \frac{1}{2} & 1 & -1 & 1 & 1 & -\frac{1}{2} & \frac{1}{2} & 1 & 1 & 1 & 1 & 1 \\ 1 & -1 & -\frac{1}{2} & 1 & 1 & -\frac{1}{2} & -1 & \frac{1}{2} & 1 & -1 & -\frac{1}{2} & 1 & \frac{1}{2} & -1 & 1 & 1 & 1 & 1 \\ 1 & -1 & 1 & -\frac{1}{2} & -1 & \frac{1}{2} & 1 & -\frac{1}{2} & -1 & 1 & \frac{1}{2} & -1 & -\frac{1}{2} & -1 & 1 & 1 & 1 & 1 \\ 1 & -\frac{1}{2} & -1 & 1 & \frac{1}{2} & -1 & 1 & -\frac{1}{2} & -1 & 1 & \frac{1}{2} & -1 & -1 & 1 & -\frac{1}{2} & 1 & 1 & 1 \\ 1 & -\frac{1}{2} & -\frac{1}{2} & 1 & -\frac{1}{2} & -1 & 1 & 1 & -1 & 1 & -1 & 1 & \frac{1}{2} & -1 & -1 & \frac{1}{2} & 1 & 1 \\ 1 & -\frac{1}{2} & -\frac{1}{2} & 1 & -1 & 1 & -1 & \frac{1}{2} & \frac{1}{2} & -1 & 1 & -1 & 1 & -1 & 1 & -1 & \frac{1}{2} & 1 \\ 1 & -1 & \frac{1}{2} & -1 & 1 & -\frac{1}{2} & -\frac{1}{2} & 1 & -1 & 1 & -\frac{1}{2} & 1 & -\frac{1}{2} & 1 & -1 & \frac{1}{2} & -1 & 1 \\ 1 & -1 & \frac{1}{2} & -\frac{1}{2} & 1 & 1 & -1 & -\frac{1}{2} & \frac{1}{2} & -1 & \frac{1}{2} & -1 & 1 & -1 & 1 & -1 & \frac{1}{2} & -1 \\ 1 & -1 & 1 & -\frac{1}{2} & \frac{1}{2} & -\frac{1}{2} & 1 & -1 & 1 & -1 & 1 & -1 & 1 & -1 & 1 & -1 & 1 & -\frac{1}{2} \end{bmatrix},$$

$$\mathbf{E}_2 = j \cdot \begin{bmatrix} -1 & 1 & -1 & 1 & -1 & 1 & -1 & 1 & -\frac{1}{2} & \frac{1}{2} & -\frac{1}{2} & \frac{1}{2} & -\frac{1}{2} \\ 1 & -1 & 1 & -\frac{1}{2} & & -\frac{1}{2} & \frac{1}{2} & -1 & 1 & -1 & 1 & -1 & \frac{1}{2} & -\frac{1}{2} \\ -1 & 1 & -\frac{1}{2} & & \frac{1}{2} & -1 & 1 & -1 & \frac{1}{2} & -\frac{1}{2} & 1 & -1 & 1 & -\frac{1}{2} \\ 1 & -\frac{1}{2} & & 1 & -1 & 1 & -\frac{1}{2} & 1 & -1 & \frac{1}{2} & \frac{1}{2} & -1 & 1 & -\frac{1}{2} \\ -1 & & \frac{1}{2} & -1 & \frac{1}{2} & \frac{1}{2} & -1 & 1 & -1 & 1 & -\frac{1}{2} & -\frac{1}{2} & 1 & -1 \\ 1 & -1 & 1 & \frac{1}{2} & -1 & \frac{1}{2} & \frac{1}{2} & -1 & \frac{1}{2} & \frac{1}{2} & -1 & 1 & -1 & \\ -1 & -\frac{1}{2} & 1 & -1 & \frac{1}{2} & \frac{1}{2} & -1 & & 1 & -\frac{1}{2} & -1 & 1 & \frac{1}{2} & -1 \\ 1 & \frac{1}{2} & -1 & -\frac{1}{2} & 1 & \frac{1}{2} & -1 & -\frac{1}{2} & 1 & \frac{1}{2} & -1 & 1 & -1 & \\ -\frac{1}{2} & -1 & \frac{1}{2} & 1 & -1 & & 1 & \frac{1}{2} & -1 & -1 & \frac{1}{2} & 1 & -\frac{1}{2} & -1 \\ \frac{1}{2} & 1 & -1 & -1 & \frac{1}{2} & 1 & \frac{1}{2} & -1 & -1 & & 1 & \frac{1}{2} & -\frac{1}{2} & -1 \\ -\frac{1}{2} & -1 & -\frac{1}{2} & \frac{1}{2} & 1 & \frac{1}{2} & -\frac{1}{2} & -1 & -1 & & 1 & 1 & -1 & -1 \\ \frac{1}{2} & 1 & 1 & \frac{1}{2} & -\frac{1}{2} & -1 & -1 & & \frac{1}{2} & 1 & 1 & -\frac{1}{2} & -1 & -1 \\ -\frac{1}{2} & -1 & -1 & -1 & -\frac{1}{2} & 1 & 1 & 1 & \frac{1}{2} & -\frac{1}{2} & -1 & -1 & -1 & -\frac{1}{2} \\ \frac{1}{2} & 1 & 1 & 1 & 1 & \frac{1}{2} & -\frac{1}{2} & -\frac{1}{2} & -1 & -1 & -1 & -1 & -1 & -\frac{1}{2} \\ -\frac{1}{2} & -\frac{1}{2} & -\frac{1}{2} & -1 & -1 & -1 & -1 & -1 & -1 & -1 & -1 & -1 & -1 & -1 & -\frac{1}{2} \end{bmatrix}.$$

The matrix  $\mathbf{A}_3$  requires only 60 real additions, while  $\mathbf{C}_3$  needs 780 real additions and 300 bit-shifting operations.

The direct implementation of the  $\mathbf{T}_{31}^*$  requires 3180 additions and 1200 bit-shifting operations. After applying the factorization in (31), the number of arithmetic operations is reduced to 900 real additions and 300 bit-shifting operations. The scaling to  $\mathbf{F}_{31}^*$  requires 60 multiplications, whereas  $\mathbf{F}'_{31}$  needs 120 additions and 120 bit-shifting operations.

#### 6.4 1023-point DFT Approximation

The PFA computation of the 1023-point DFT, as defined in Section 2.2, requires  $(33 \times 2700) + (93 \times 300) + (341 \times 12) = 121092$  real multiplications, and  $(33 \times 4560) + (93 \times 520) + (341 \times 24) = 207024$  real additions using the 3-, 11-, and 31-point DFTs directly from their definitions. However, if the exact 1023-point DFT is computed by the sparse matrix factorizations detailed in Appendix A, then  $(33 \times 900) + (93 \times 100) + (341 \times 2) = 39682$  real multiplications,  $(33 \times 1020) + (93 \times 140) + (341 \times 12) = 50772$  real additions, and  $(341 \times 2) = 682$  bit-shifting operations are needed.

The unscaled algorithm to compute the 1023-point DFT approximation, referred to as  $\hat{\mathbf{T}}_{1023}^*$ , has null complexity of multiplications. To calculate  $\hat{\mathbf{T}}_{1023}^*$ , the matrix  $\mathbf{T}_{31}^*$  is called 33 times contributing with  $900 \times 33 = 29700$  real additions and  $300 \times 33 = 9900$  bit-shifting operations. On the other hand,  $\mathbf{T}_{11}^*$  is called 93 times contributing with  $130 \times 93 = 12090$  real additions and  $40 \times 93 = 3720$  bit-shifting operations and  $\mathbf{T}_3^*$  is called 341 times which corresponds to  $12 \times 341 = 4092$  real additions and  $2 \times 341 = 682$  bit-shifting operations. Then, the resulting arithmetic costs of  $\hat{\mathbf{T}}_{1023}^*$  are 45882 real additions and 14302 bit-shifting operations. To compute the scaled 1023-point DFT approximation with the exact  $\mathbf{S}$ , called  $\hat{\mathbf{F}}_{1023}^*$ , more 2044 multiplications are necessary. However, if  $\mathbf{S}$  is approximated following Table 1, instead of multiplications, 4088 additions and 4088 bit-shifting operations are needed to achieve  $\hat{\mathbf{F}}'_{1023}$ .

#### 6.5 Hybrid 1023-point DFT Approximation

Applying the hybrid approach detailed in Section 4.3 to the 1023-point DFT approximation defined in (24) and (25), we obtained 12 distinct approximations. The 1023-point DFT approximations consist of four elements: a diagonal matrix  $\hat{\mathbf{S}}$ , a 3-, an 11-, and a 31-point transformation. In the hybrid approximations, these four elements are alternated between exact and approximate form. Table 2 helps to understand the approximations by providing the combinations of the these four elements. The computation of the exact DFT was performed according to the algorithms detailed in the Appendix A.

The arithmetic complexity of the 1023-point DFT approximations is summarized in Table 4 and can be obtained using

Table 2: Hybrid Approximations for the 1023-point DFT

Approximation	$\hat{\mathbf{S}}$	Employed transformation		
		3-point	11-point	31-point
$\hat{\mathbf{F}}_{1023,I}^*$	Exact	$\mathbf{T}_3^*$	$\mathbf{F}_{11}$	$\mathbf{F}_{31}$
$\hat{\mathbf{F}}'_{1023,I}$	CSD approx.	$\mathbf{T}_3^*$	$\mathbf{F}_{11}$	$\mathbf{F}_{31}$
$\hat{\mathbf{F}}_{1023,II}^*$	Exact	$\mathbf{F}_3$	$\mathbf{T}_{11}^*$	$\mathbf{F}_{31}$
$\hat{\mathbf{F}}'_{1023,II}$	CSD approx.	$\mathbf{F}_3$	$\mathbf{T}_{11}^*$	$\mathbf{F}_{31}$
$\hat{\mathbf{F}}_{1023,III}^*$	Exact	$\mathbf{T}_3^*$	$\mathbf{T}_{11}^*$	$\mathbf{F}_{31}$
$\hat{\mathbf{F}}'_{1023,III}$	CSD approx.	$\mathbf{T}_3^*$	$\mathbf{T}_{11}^*$	$\mathbf{F}_{31}$
$\hat{\mathbf{F}}_{1023,IV}^*$	Exact	$\mathbf{F}_3$	$\mathbf{F}_{11}$	$\mathbf{T}_{31}^*$
$\hat{\mathbf{F}}'_{1023,IV}$	CSD approx.	$\mathbf{F}_3$	$\mathbf{F}_{11}$	$\mathbf{T}_{31}^*$
$\hat{\mathbf{F}}_{1023,V}^*$	Exact	$\mathbf{T}_3^*$	$\mathbf{F}_{11}$	$\mathbf{T}_{31}^*$
$\hat{\mathbf{F}}'_{1023,V}$	CSD approx.	$\mathbf{T}_3^*$	$\mathbf{F}_{11}$	$\mathbf{T}_{31}^*$
$\hat{\mathbf{F}}_{1023,VI}^*$	Exact	$\mathbf{F}_3$	$\mathbf{T}_{11}^*$	$\mathbf{T}_{31}^*$
$\hat{\mathbf{F}}'_{1023,VI}$	CSD approx.	$\mathbf{F}_3$	$\mathbf{T}_{11}^*$	$\mathbf{T}_{31}^*$

the following equation:

$$\begin{aligned}
 \mathcal{A}(1023\text{-point DFT}) = & \mathcal{A}(\hat{\mathbf{S}}) + 33 \cdot \mathcal{A}(31\text{-point DFT}) \\
 & + 93 \cdot \mathcal{A}(11\text{-point DFT}), \\
 & + 341 \cdot \mathcal{A}(3\text{-point DFT})
 \end{aligned} \tag{32}$$

where  $\mathcal{A}(\cdot)$  represents the arithmetic complexity of the argument, including operations such as multiplications, additions, and bit-shifting.

## 7 Comparison and Discussion

In this section, we assess and compare the proposed methods with competing methods. The comparisons encompass: arithmetic complexity, error analysis, and frequency response.

### 7.1 Arithmetic Complexity

#### 7.1.1 Complexity Measurements

Table 3 shows the arithmetic complexity of the proposed ground transformation matrices compared with: (i) their respective exact counterparts, (ii) the ground transformation used in [53] denoted by  $\hat{\mathbf{F}}_{32}$ , and (iii) the exact 32-point DFT calculated by the fully optimized Cooley-Tukey Radix-2 [6] denoted by  $\mathbf{F}_{32}$ .

In Table 4, we compare the arithmetic complexity of the proposed 1023-point DFT approximation algorithm with (i) the 1023-point exact DFT computed by the prime factor algorithm without fast algorithms for the ground transforms; (ii) the 1023-point exact DFT computed by the prime factor algorithm with fast algorithms for the ground transforms; (iii) the 1024-point exact DFT computed by definition ( $\mathbf{F}_{1024}$ ); (iv) the 1024-point exact DFT computed by the fully optimized Cooley-Tukey Radix-2 ( $\mathbf{F}_{1024}$ ); and (iv) the fast algorithms for the 1024-point DFT approximation— $\hat{\mathbf{F}}_{1024}^I$ ,  $\hat{\mathbf{F}}_{1024}^{II}$ , and  $\hat{\mathbf{F}}_{1024}^{III}$ —proposed in [53]. Such methods are the closest comparable algorithms in the literature. In  $\hat{\mathbf{F}}_{1024}^I$ , both row- and column-wise 32-point DFTs are replaced by the multiplierless  $\hat{\mathbf{F}}_{32}$  [20]. In  $\hat{\mathbf{F}}_{1024}^{II}$  and  $\hat{\mathbf{F}}_{1024}^{III}$ , either the column- or row-wise operation is kept in the exact form.

Table 3: Arithmetic Complexity of the Approximate Ground Transforms and Comparison

$N$	Transform	Real Mult.	Real Add.	Bit-shifting
3	$\mathbf{F}_3$ (by definition [64])	12	24	0
	$\mathbf{F}_3$ (by the proposed FFT)	2	12	2
	$\hat{\mathbf{T}}_3^*$	0	12	2
	$\hat{\mathbf{F}}_3^*$	4	12	2
	$\hat{\mathbf{F}}_3'$	0	20	10
11	$\mathbf{F}_{11}$ (by definition [64])	300	520	0
	$\mathbf{F}_{11}$ (by the proposed FFT)	100	140	0
	$\hat{\mathbf{T}}_{11}^*$	0	130	40
	$\hat{\mathbf{F}}_{11}^*$	20	130	40
	$\hat{\mathbf{F}}_{11}'$	0	170	80
31	$\mathbf{F}_{31}$ (by definition [64])	2700	4560	0
	$\mathbf{F}_{31}$ (by the proposed FFT)	900	1020	0
	$\hat{\mathbf{T}}_{31}^*$	0	900	300
	$\hat{\mathbf{F}}_{31}^*$	60	900	300
	$\hat{\mathbf{F}}_{31}'$	0	1020	420
32	$\mathbf{F}_{32}$ (Cooley-Tukey Radix-2 [6])	88	408	0
	$\hat{\mathbf{F}}_{32}$ (proposed in [53])	0	348	0

Table 4: Arithmetic Complexity Assessment and Comparison

$N$	Transform	Real Mult.	Real Add.	Bit-shifting
1023	$\mathbf{F}_{1023}$ (PFA) [64])	121092	207024	0
	$\mathbf{F}_{1023}$ (PFA and fast algorithms)	39682	50772	682
	$\hat{\mathbf{F}}_{1023,I}^*$	40364	50772	682
	$\hat{\mathbf{F}}_{1023,I}'$	39000	53500	3410
	$\hat{\mathbf{F}}_{1023,II}^*$	32242	49842	4402
	$\hat{\mathbf{F}}_{1023,II}'$	30382	53562	8122
	$\hat{\mathbf{F}}_{1023,III}^*$	11962	46812	10582
	$\hat{\mathbf{F}}_{1023,III}'$	9982	50772	14542
	$\hat{\mathbf{F}}_{1023,IV}^*$	31684	49842	4402
	$\hat{\mathbf{F}}_{1023,IV}'$	29700	53810	8370
	$\hat{\mathbf{F}}_{1023,V}^*$	11324	46812	10582
	$\hat{\mathbf{F}}_{1023,V}'$	9300	50860	14630
	$\hat{\mathbf{F}}_{1023,VI}^*$	2722	45882	14302
	$\hat{\mathbf{F}}_{1023,VI}'$	682	49962	18382
1024	$\hat{\mathbf{T}}_{1023}^*$	0	45882	14302
	$\hat{\mathbf{F}}_{1023}^*$	2044	45882	14302
	$\hat{\mathbf{F}}_{1023}'$	<b>0</b>	<b>49970</b>	<b>18390</b>
	$\mathbf{F}_{1024}$ (exact, by definition [6])	3084288	5159936	0
	$\mathbf{F}_{1024}$ (Cooley-Tukey [6])	10248	30728	0
1024	$\hat{\mathbf{F}}_{1024}^I$ (proposed in [53])	2883	25155	0
	$\hat{\mathbf{F}}_{1024}^{II}$ (proposed in [53])	5699	27075	0
	$\hat{\mathbf{F}}_{1024}^{III}$ (proposed in [53])	5699	27075	0

Table 5: Error Measurements of the Ground Approximate Transforms

$N$	Transform	$\epsilon$	$M$	$\phi \times 10^3$
3	$\hat{\mathbf{F}}_3^*$	0.0968	1.59	6.73
	$\hat{\mathbf{F}}_3'$	0.0975	1.60	6.77
11	$\hat{\mathbf{F}}_{11}^*$	8.88	1.19	14.12
	$\hat{\mathbf{F}}_{11}'$	8.90	1.20	14.11
31	$\hat{\mathbf{F}}_{31}^*$	76.60	0.45	19.83
	$\hat{\mathbf{F}}_{31}'$	76.90	0.45	19.84
32	$\hat{\mathbf{F}}_{32}$	332	0.84	36.07

### 7.1.2 Discussion

Table 3 shows that power-of-two ground transformation matrices benefit more from factorization than prime-length transformations. However, when ground transforms are used as a building block to derive larger transforms, a different phenomenon occurs. Indeed, the  $N$  complex multiplications due to the twiddle factors present in Cooley-Tukey-based approximations offset the complexity reductions from its factorization. In contrast, the proposed PFA-based approximations do not require intermediate multiplications by twiddle factors. In particular, the proposed approximations  $\hat{\mathbf{T}}_{1023}^*$  and  $\hat{\mathbf{F}}_{1023}'$  are entirely multiplierless.

This feature has a direct impact on hardware efficiency. As a reference, the approximation with the lowest arithmetic complexity proposed in [53] ( $\hat{\mathbf{F}}_{1024}^I$ ) achieved reductions of up to 48.5% in chip area, 30% in critical path delay (CPD), and 66.0% in energy consumption compared to the conventional radix-2 Cooley-Tukey FFT implementation. Given that the proposed approximations  $\hat{\mathbf{T}}_{1023}^*$  and  $\hat{\mathbf{F}}_{1023}'$  require no multiplications, it is therefore reasonable to expect that the proposed method could achieve at least comparable reductions in terms of power consumption, chip area, and CPD.

## 7.2 Error Analysis

Table 5 and 6 summarize the proximity measurements (Section 3.2) for the proposed approximations compared the approximations proposed in [20,53]. Although the proposed approximations are not strictly orthogonal, their deviations from orthogonality are extremely low ( $\approx 10^{-2}$ ). MAPE measurements are also smaller for the proposed approximations. The total error energy ( $\epsilon$ ) indicates that the proposed approximations are more refined than the approximations in [20,53]. The good performance of the proposed ground approximations is transferred to the 1023-point DFT approximations.

The applicability of approximate DFTs to practical scenarios such as digital beamforming and spectrum sensing has been demonstrated in [20,53]. In both cases, the adopted approximations proved adequate for real-world implementations despite presenting higher error levels compared to the methods proposed in this work. Therefore, given that blocklength is not a critical constraint in these contexts and that the proposed approximations achieve even lower error rates, it is reasonable to expect that they are equally, if not more, suitable for these classes of applications, while fully eliminating multiplications.

## 7.3 Frequency Response

Considering the rows of the linear transform matrix as a finite impulse response (FIR) filter bank [64], it is possible to evaluate the approximation performance according to the frequency response of the considered filters. This approach is justified by the fact that, in linear time-invariant systems, any input signal can be expressed as a linear combination of shifted impulses [59]. In this way, analyzing the impulse response of each row provides a complete and interpretable characterization of the transformation behavior.

Table 6: Error Measurements of the Proposed 1023-point Approximation and Comparison

$N$	Transform	$\epsilon \times 10^{-4}$	$M \times 10^3$	$\phi \times 10^3$
1023	$\hat{\mathbf{F}}_{1023,\text{I}}^*$	1.13	4.67	6.73
	$\hat{\mathbf{F}}_{1023,\text{I}}'$	1.13	4.69	6.77
	$\hat{\mathbf{F}}_{1023,\text{II}}^*$	7.68	12.83	14.12
	$\hat{\mathbf{F}}_{1023,\text{II}}'$	7.70	12.86	14.11
	$\hat{\mathbf{F}}_{1023,\text{III}}^*$	8.35	13.68	19.83
	$\hat{\mathbf{F}}_{1023,\text{III}}'$	8.38	13.70	19.84
	$\hat{\mathbf{F}}_{1023,\text{IV}}^*$	8.80	14.12	20.76
	$\hat{\mathbf{F}}_{1023,\text{IV}}'$	8.88	14.18	20.79
	$\hat{\mathbf{F}}_{1023,\text{V}}^*$	9.46	14.77	26.43
	$\hat{\mathbf{F}}_{1023,\text{V}}'$	9.55	14.82	26.49
	$\hat{\mathbf{F}}_{1023,\text{VI}}^*$	15.93	18.67	33.68
	$\hat{\mathbf{F}}_{1023,\text{VI}}'$	16.66	19.86	33.78
	$\hat{\mathbf{F}}_{1023}^*$	17.03	19.41	40.18
	$\hat{\mathbf{F}}_{1023}'$	17.10	19.45	40.06
1024	$\hat{\mathbf{F}}_{1024}^{\text{I}}$	93.00	44	69.42
	$\hat{\mathbf{F}}_{1024}^{\text{II}}$	34.02	25.31	36.07
	$\hat{\mathbf{F}}_{1024}^{\text{III}}$	34.02	25.31	36.07

The analysis is focused on  $\hat{\mathbf{F}}_3'$ ,  $\hat{\mathbf{F}}_{11}'$ ,  $\hat{\mathbf{F}}_{31}'$ , and  $\hat{\mathbf{F}}_{1023}'$  because they are fully approximated, scaled, and free of multiplications.

### 7.3.1 Overall Assessment

The frequency response error energy ( $\epsilon$ ) measurements for  $\hat{\mathbf{F}}_3'$ ,  $\hat{\mathbf{F}}_{11}'$ , and  $\hat{\mathbf{F}}_{31}'$  relative to the exact filter bank are given in Table 7. The lowest measurements are in boldface.

Fig. 1(a)–(d) shows the error energy for all filters from the 3-, 11-, 31-, and 1023-point approximations. Each row of the transform matrix is interpreted as a FIR filter and is represented by a distinct color in the plot. The vertical axis corresponds to the normalized magnitude response in decibels (dB), computed as:

$$20\log_{10}\left(\frac{|H(\omega)|}{\max_{\omega}|H(\omega)|}\right),$$

where  $H(\omega)$  is the frequency response of the row under analysis. This normalization sets the main lobe peak at 0dB, allowing for visual inspection of attenuation and spectral leakage across frequencies. Although the curves appear visually similar to each other, it is still possible to observe that the error is kept under  $-17$  dB in all cases. In [53], the approximations  $\hat{\mathbf{F}}_{1024}^{\text{I}}$ ,  $\hat{\mathbf{F}}_{1024}^{\text{II}}$ , and  $\hat{\mathbf{F}}_{1024}^{\text{III}}$  produced errors below  $-6.8$  dB,  $-11.52$  dB, and  $-10.61$  dB, respectively.

Notice that, for all proposed approximations (see Table 7), including those with blocklength 1023 derived from the PFA, the DC component remains unchanged and is computed exactly as in the exact DFT. This holds because neither the approximation procedure nor the orthogonalization process modifies the 0th row of the DFT matrix, which is solely composed of ones and inherently has low-complexity. Therefore, the approximation error is exclusively associated with the non-DC frequency components, while the DC level remains identical to the one calculated by exact DFT. In addition, an analysis is presented for the frequency response to a pure cosine input generated by

$$x[n] = \cos\left(2\pi \cdot \frac{100}{N} \cdot n\right), \quad n = 0, 1, \dots, N-1. \quad (33)$$

Table 7: Error Energy of 3-, 11-, and 31-point DFT approximations (least performing are highlighted)

Method	Row											Total				
	1	2	3	4	5	6	7	8	9	10	11					
$\hat{\mathbf{F}}'_3$	<b>0.00</b>	<b>0.08</b>	<b>0.01</b>									0.09				
$\hat{\mathbf{F}}'_{11}$	0.00	0.44	1.01	0.93	<b>1.09</b>	<b>1.33</b>	0.46	0.69	0.85	0.77	<b>1.34</b>	8.90				
Method	Row											Total				
	1	2	3	4	5	6	7	8	9	10	11					
	0.00	2.08	2.91	1.56	<b>3.66</b>	1.97	<b>3.69</b>	3.26	0.82	3.36	1.56	3.38	2.54	1.60	2.73	1.91
$\hat{\mathbf{F}}'_{31}$	17	18	19	20	21	22	23	24	25	26	27	28	29	30	31	76.8
	3.20	2.38	3.51	2.57	1.73	3.56	1.77	<b>4.29</b>	1.87	1.45	3.16	1.47	3.55	2.22	3.04	

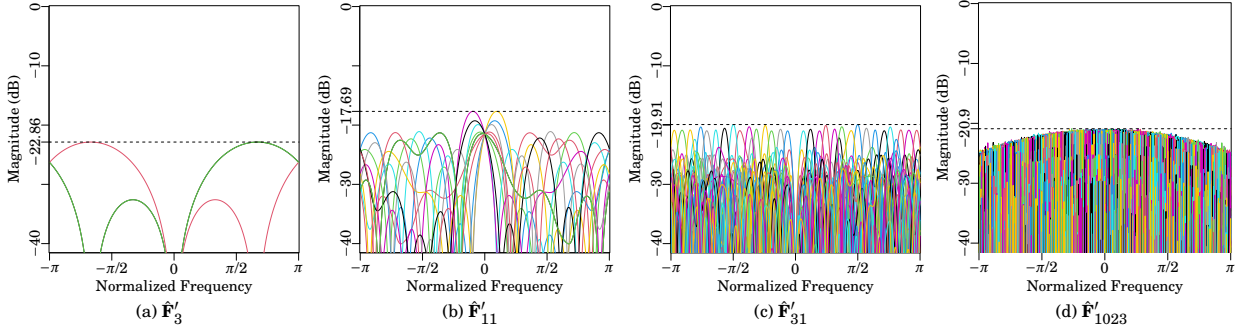


Figure 1: Error plots between the filter bank frequency response magnitude for (a) 3-point approximation, (b) 11-point approximation, (c) 31-point approximation, and (d) 1023-point approximation and their exact counterparts.

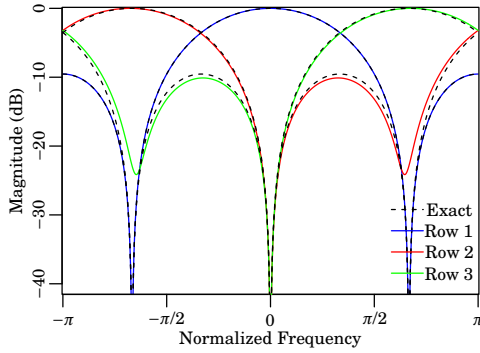
Fig. 4 presents the magnitude responses obtained by applying the exact and DFT approximations to a pure cosine signal, where the dashed line represents the maximum value of the non-dominant frequencies. In this analysis, the results are shown in linear scale (rather than in dB) to improve visualization. As shown in Fig. 4(a), the approximation  $\hat{\mathbf{F}}'_{1024}$  exhibits noticeable leakage across several non-dominant frequencies, along with distortion in one of the main lobes (left side). In the hybrid approximation  $\hat{\mathbf{F}}''_{1024}$ , in Fig. 4(b), the leakage in non-dominant frequencies is reduced but distortion in the left main lobe remains. In Fig. 4(c), the hybrid approximation  $\hat{\mathbf{F}}'''_{1024}$  presents the main lobes close to their exact counterparts, but it presents leakage in more non-dominant frequencies than  $\hat{\mathbf{F}}''_{1024}$ . In contrast, the proposed approximation  $\hat{\mathbf{F}}'_{1023}$ , shown in Fig. 4(d), achieves a closer match to the exact DFT in the main lobes and a lower maximum leakage in non-dominant frequencies.

### 7.3.2 Worst-case Scenario

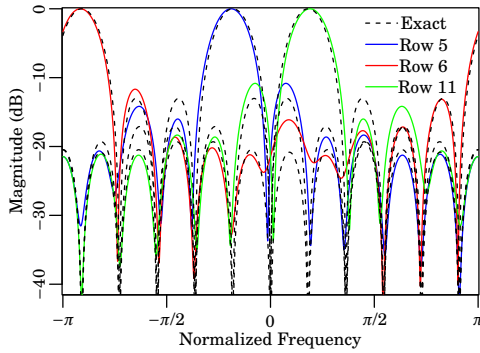
Fig. 2(a)–(c) displays the frequency response magnitude plots of the three least-performing filters for the ground 3-, 11-, and 31-point approximations compared with their exact counterparts, respectively.

Fig. 3(a)–(c) address the 1023-point approximation and shows the frequency response magnitude plot associated to matrix rows (filters) 86, 699, and 854, respectively. These are the least performing filters, presenting error energy measurements of 306.08, 287.1, and 286.29, respectively; being 167.15 the average error energy from all filters.

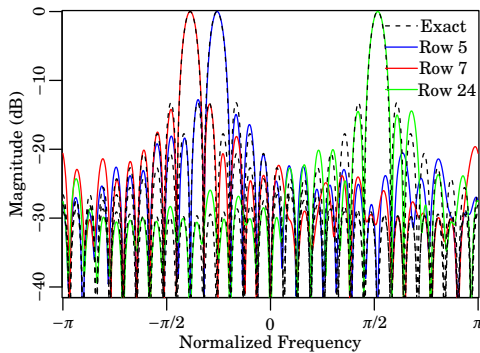
Even under such worst-case scenario analysis, the approximate methods were able to preserve the main and the secondary lobes from the exact DFT.



(a)  $\hat{\mathbf{F}}'_3$



(b)  $\hat{\mathbf{F}}'_11$



(c)  $\hat{\mathbf{F}}'_11$

Figure 2: Comparison between the magnitude of the filter-bank responses of the approximations and their exact counterparts for the least three performing rows.

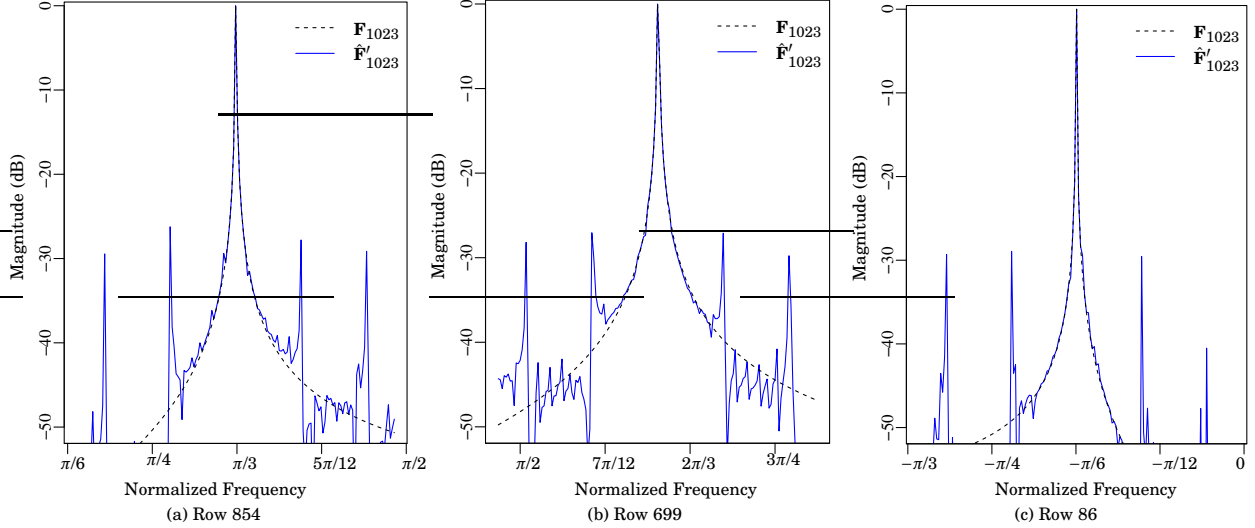


Figure 3: Comparison between the magnitude of the filter-bank responses of the approximation  $\hat{\mathbf{F}}'_{1023}$  and the exact DFT for the least three performing rows.

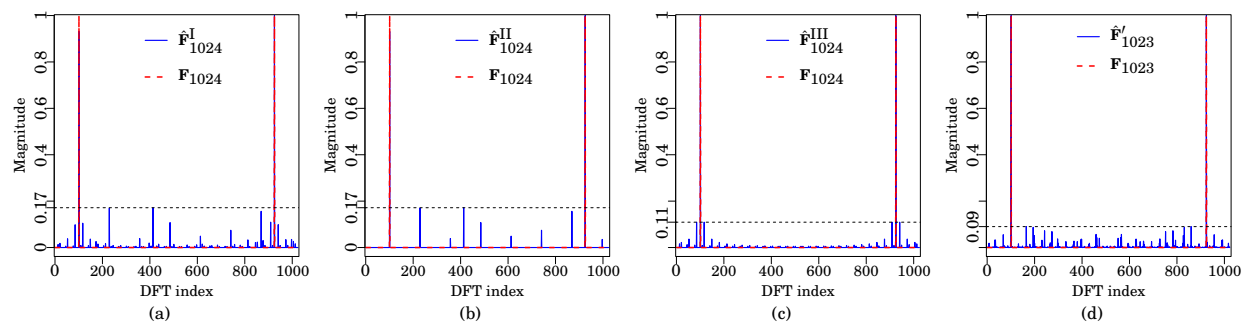


Figure 4: Comparison between the magnitude responses obtained from [53] and  $\hat{\mathbf{F}}'_{1023}$  with their exact counterparts, applied to a pure cosine signal.

## 8 Conclusion

In this paper, we proposed a method to obtain matrices with null multiplicative complexity on the prime factor algorithm. We demonstrated that, if the transform length can be decomposed into relatively prime numbers, then the entire approximate DFT computation can be performed multiplierlessly. The absence of twiddle factors simplifies the design when compared to Cooley-Tukey-based approximations and also reduces the error propagation from the approximate ground transforms. We applied the proposed method to derive a 1023-point DFT approximation along with a collection of approximations, trading-off accuracy for computational cost and vice-versa. The proposed method outperformed the comparable methods in the literature according to popular figures of merit.

The main contributions of this paper are summarized as follows:

- A generic method to obtain multiplierless DFT approximations using the prime factor algorithm;
- Three novel approximations for the 3-point DFT;
- Three novel approximations for the 11-point DFT;
- Three novel approximations for the 31-point DFT;
- A procedure to construct large multiplierless DFT approximations when the transform length can be decomposed into relatively prime factors;
- Fifteen approximations for the 1023-point DFT, derived using the proposed method.

For future work, we aim to extend this framework to different blocklengths. Preliminary results for the 65-point DFT ( $65 = 5 \times 13$ ) have already corroborated the scalability and consistency of the method, preserving its fully multiplierless and low-complexity characteristics. In particular, large transform sizes that result from coprime factorizations—such as 2046 ( $2 \times 3 \times 11 \times 31$ )—which directly benefits from the results and approximations developed in this work. Additionally, practical hardware implementations of the proposed method is sought to be investigated. In this context, we highlight memory-efficient strategies such as in-place and in-order computation. As shown in [51], such techniques are directly possible in PFA algorithms only when the transform blocklength prime factors are quadratic residues of each other. However, an earlier work by [14] introduced a variation of the PFA that enables fully in-place and in-order execution for arbitrary factorizations. This approach significantly reduces memory usage, eliminates the need for post-processing (unscrambling), and may achieve faster computation than traditional FFT algorithms such as Cooley-Tukey radix-4.

## A Fast Algorithms for the Exact Transforms

This appendix discusses the arithmetic complexity and provides fast algorithms for the exact 3-, 11-, and 31-point DFT. The resulting arithmetic complexity is shown in Table 3.

### A.1 3-, 11-, and 31-point DFT

The direct computation of the DFT requires complex multiplications in the order of  $\mathcal{O}(N^2)$  [64]. Therefore, disregarding the trivial multipliers, if we consider a complex input, the direct computation of the 3-, 11-, and 31-point DFT requires 12 real multiplications and 24 real additions; 300 real multiplications and 520 real additions; and 2700 real multiplications and 4560 real additions, respectively.

## A.2 Fast Algorithms

### A.2.1 3-point DFT

Matrix  $\mathbf{F}_3$  can be factorized as:

$$\mathbf{F}_3 = \mathbf{A}_1^\top \cdot \begin{bmatrix} 1 & 1 \\ 1 & -\frac{1}{2} \\ & \frac{-j\sqrt{3}}{2} \end{bmatrix} \cdot \mathbf{A}_1. \quad (34)$$

### A.2.2 11-point DFT

Let  $\beta_x = \cos\left(\frac{x\pi}{N}\right)$  and  $\delta_x = j \cdot \sin\left(\frac{x\pi}{N}\right)$ . Matrix  $\mathbf{F}_{11}$  can be represented as:

$$\mathbf{F}_{11} = \mathbf{A}_2^\top \cdot \begin{bmatrix} 1 & 1 & 1 & 1 & 1 & 1 \\ 1 & \beta_2 & \beta_4 & \beta_6 & \beta_8 & \beta_{10} \\ 1 & \beta_4 & \beta_8 & \beta_{10} & \beta_6 & \beta_2 \\ 1 & \beta_6 & \beta_{10} & \beta_4 & \beta_2 & \beta_8 \\ 1 & \beta_8 & \beta_6 & \beta_2 & \beta_{10} & \beta_4 \\ 1 & \beta_{10} & \beta_2 & \beta_8 & \beta_4 & \beta_6 \end{bmatrix} \cdot \mathbf{A}_2. \quad (35)$$

### A.2.3 31-point DFT

Matrix  $\mathbf{F}_{31}$  can be expressed as:

$$\mathbf{F}_{31} = \mathbf{A}_3^\top \cdot \begin{bmatrix} \mathbf{E}_3 & \mathbf{E}_4 \end{bmatrix} \cdot \mathbf{A}_3, \quad (36)$$

where

$$\mathbf{E}_3 = \begin{bmatrix} 1 & 1 & 1 & 1 & 1 & 1 & 1 & 1 & 1 & 1 & 1 & 1 & 1 & 1 & 1 & 1 \\ 1 & \beta_2 & \beta_4 & \beta_6 & \beta_8 & \beta_{10} & \beta_{12} & \beta_{14} & \beta_{16} & \beta_{18} & \beta_{20} & \beta_{22} & \beta_{24} & \beta_{26} & \beta_{28} & \beta_{30} \\ 1 & \beta_4 & \beta_8 & \beta_{12} & \beta_{16} & \beta_{20} & \beta_{24} & \beta_{28} & \beta_{30} & \beta_{26} & \beta_{22} & \beta_{18} & \beta_{14} & \beta_{10} & \beta_6 & \beta_2 \\ 1 & \beta_6 & \beta_{12} & \beta_{18} & \beta_{24} & \beta_{30} & \beta_{26} & \beta_{20} & \beta_{14} & \beta_8 & \beta_2 & \beta_4 & \beta_{10} & \beta_{16} & \beta_{22} & \beta_{28} \\ 1 & \beta_8 & \beta_{16} & \beta_{24} & \beta_{30} & \beta_{22} & \beta_{14} & \beta_6 & \beta_2 & \beta_{10} & \beta_{18} & \beta_{26} & \beta_{28} & \beta_{20} & \beta_{12} & \beta_4 \\ 1 & \beta_{10} & \beta_{20} & \beta_{30} & \beta_{22} & \beta_{12} & \beta_2 & \beta_8 & \beta_{18} & \beta_{28} & \beta_{24} & \beta_{14} & \beta_4 & \beta_6 & \beta_{16} & \beta_{26} \\ 1 & \beta_{12} & \beta_{24} & \beta_{26} & \beta_{14} & \beta_2 & \beta_{10} & \beta_{22} & \beta_{28} & \beta_{16} & \beta_4 & \beta_8 & \beta_{20} & \beta_{30} & \beta_{18} & \beta_6 \\ 1 & \beta_{14} & \beta_{28} & \beta_{20} & \beta_6 & \beta_8 & \beta_{22} & \beta_{26} & \beta_{12} & \beta_2 & \beta_{16} & \beta_{30} & \beta_{18} & \beta_4 & \beta_{10} & \beta_{24} \\ 1 & \beta_{16} & \beta_{30} & \beta_{14} & \beta_2 & \beta_{18} & \beta_{28} & \beta_{12} & \beta_4 & \beta_{20} & \beta_{26} & \beta_{10} & \beta_6 & \beta_{22} & \beta_{24} & \beta_8 \\ 1 & \beta_{18} & \beta_{26} & \beta_8 & \beta_{10} & \beta_{28} & \beta_{16} & \beta_2 & \beta_{20} & \beta_{24} & \beta_6 & \beta_{12} & \beta_{30} & \beta_{14} & \beta_4 & \beta_{22} \\ 1 & \beta_{20} & \beta_{22} & \beta_2 & \beta_{18} & \beta_{24} & \beta_4 & \beta_{16} & \beta_{26} & \beta_6 & \beta_{14} & \beta_{28} & \beta_8 & \beta_{12} & \beta_{30} & \beta_{10} \\ 1 & \beta_{22} & \beta_{18} & \beta_4 & \beta_{26} & \beta_{14} & \beta_8 & \beta_{30} & \beta_{10} & \beta_{12} & \beta_{28} & \beta_6 & \beta_{16} & \beta_{24} & \beta_2 & \beta_{20} \\ 1 & \beta_{24} & \beta_{14} & \beta_{16} & \beta_{28} & \beta_4 & \beta_{20} & \beta_{18} & \beta_6 & \beta_{30} & \beta_8 & \beta_{16} & \beta_{22} & \beta_2 & \beta_{24} & \beta_{12} \\ 1 & \beta_{26} & \beta_{10} & \beta_{16} & \beta_{20} & \beta_6 & \beta_{30} & \beta_4 & \beta_{22} & \beta_{14} & \beta_{12} & \beta_{24} & \beta_2 & \beta_{28} & \beta_8 & \beta_{18} \\ 1 & \beta_{28} & \beta_6 & \beta_{22} & \beta_{12} & \beta_{16} & \beta_{18} & \beta_{10} & \beta_{24} & \beta_4 & \beta_{30} & \beta_2 & \beta_{26} & \beta_8 & \beta_{20} & \beta_{14} \\ 1 & \beta_{30} & \beta_2 & \beta_{28} & \beta_4 & \beta_{26} & \beta_6 & \beta_{24} & \beta_8 & \beta_{22} & \beta_{10} & \beta_{20} & \beta_{12} & \beta_{18} & \beta_{14} & \beta_{16} \end{bmatrix},$$

$$\mathbf{E}_4 = \begin{bmatrix} -\delta_{15} & \delta_{14} & -\delta_{13} & \delta_{12} & -\delta_{11} & \delta_{10} & -\delta_9 & \delta_8 & -\delta_7 & \delta_6 & -\delta_5 & \delta_4 & -\delta_3 & \delta_2 & -\delta_1 \\ \delta_{14} & -\delta_{11} & \delta_8 & -\delta_5 & \delta_2 & \delta_1 & -\delta_4 & \delta_7 & -\delta_{10} & \delta_{13} & -\delta_{15} & \delta_{12} & -\delta_9 & \delta_6 & -\delta_3 \\ -\delta_{13} & \delta_8 & -\delta_3 & -\delta_2 & \delta_7 & -\delta_{12} & \delta_{14} & -\delta_9 & \delta_4 & \delta_1 & -\delta_6 & \delta_{11} & -\delta_{15} & \delta_{10} & -\delta_5 \\ \delta_{12} & -\delta_5 & -\delta_2 & \delta_9 & -\delta_{15} & \delta_8 & -\delta_1 & -\delta_6 & \delta_{13} & -\delta_{11} & \delta_4 & \delta_3 & -\delta_{10} & \delta_{14} & -\delta_7 \\ -\delta_{11} & \delta_2 & \delta_7 & -\delta_{15} & \delta_6 & \delta_3 & -\delta_{12} & \delta_{10} & -\delta_1 & -\delta_8 & \delta_{14} & -\delta_5 & -\delta_4 & \delta_{13} & -\delta_9 \\ \delta_{10} & \delta_1 & -\delta_{12} & \delta_8 & \delta_3 & -\delta_{14} & \delta_6 & \delta_5 & -\delta_{15} & \delta_4 & \delta_7 & -\delta_{13} & \delta_2 & \delta_9 & -\delta_{11} \\ -\delta_9 & -\delta_4 & \delta_{14} & -\delta_1 & -\delta_{12} & \delta_6 & \delta_7 & -\delta_{11} & -\delta_2 & \delta_{15} & -\delta_3 & -\delta_{10} & \delta_8 & \delta_5 & -\delta_{13} \\ \delta_8 & \delta_7 & -\delta_9 & -\delta_6 & \delta_{10} & \delta_5 & -\delta_4 & \delta_{12} & \delta_3 & -\delta_{13} & -\delta_2 & \delta_{14} & \delta_1 & -\delta_{15} & . \\ -\delta_7 & -\delta_{10} & \delta_4 & \delta_{13} & -\delta_1 & -\delta_{15} & -\delta_2 & \delta_{12} & \delta_5 & -\delta_9 & -\delta_8 & \delta_6 & \delta_{11} & -\delta_3 & -\delta_{14} \\ \delta_6 & \delta_{13} & \delta_1 & -\delta_{11} & -\delta_8 & \delta_4 & \delta_{15} & \delta_3 & -\delta_9 & -\delta_{10} & \delta_2 & \delta_{14} & \delta_5 & -\delta_7 & -\delta_{12} \\ -\delta_5 & -\delta_{15} & -\delta_6 & \delta_4 & \delta_{14} & \delta_7 & -\delta_3 & -\delta_{13} & -\delta_8 & \delta_2 & \delta_{12} & \delta_9 & -\delta_1 & -\delta_{11} & -\delta_{10} \\ \delta_4 & \delta_{12} & \delta_{11} & \delta_3 & -\delta_5 & -\delta_{13} & -\delta_{10} & -\delta_2 & \delta_6 & \delta_{14} & \delta_9 & \delta_1 & -\delta_7 & -\delta_{15} & -\delta_8 \\ -\delta_3 & -\delta_9 & -\delta_{15} & -\delta_{10} & -\delta_4 & \delta_2 & \delta_8 & \delta_{14} & \delta_{11} & \delta_5 & -\delta_1 & -\delta_7 & -\delta_{13} & -\delta_{12} & -\delta_6 \\ \delta_2 & \delta_6 & \delta_{10} & \delta_{14} & \delta_{13} & \delta_9 & \delta_5 & \delta_1 & -\delta_3 & -\delta_7 & -\delta_{11} & -\delta_{15} & -\delta_{12} & -\delta_8 & -\delta_4 \\ -\delta_1 & -\delta_3 & -\delta_5 & -\delta_7 & -\delta_9 & -\delta_{11} & -\delta_{13} & -\delta_{15} & -\delta_{14} & -\delta_{12} & -\delta_{10} & -\delta_8 & -\delta_6 & -\delta_4 & -\delta_2 \end{bmatrix}.$$

## References

- [1] S. A. ALAWSH AND A. H. MUQAIBEL, *Multi-level prime array for sparse sampling*, IET Signal Processing, 12 (2018), p. 688–699.
- [2] V. ARIYARATHNA, D. F. G. COELHO, S. PULIPATI, R. J. CINTRA, F. M. BAYER, V. S. DIMITROV, AND A. MADANAYAKE, *Multibeam digital array receiver using a 16-point multiplierless DFT approximation*, IEEE Transactions on Antennas and Propagation, 67 (2018), p. 925–933.
- [3] A. AVIZIENIS, *Signed-digit number representations for fast parallel arithmetic*, IRE Transactions on Electronic Computers, EC-10 (1961), p. 389–400.
- [4] V. BARICHARD, X. GANDIBLEUX, AND V. T'KINDT, *Multiobjective programming and goal programming: theoretical results and practical applications*, vol. 618, Springer Science & Business Media, Heidelberg, BW, 2008.
- [5] F. M. BAYER AND R. J. CINTRA, *DCT-like transform for image compression requires 14 additions only*, Electronics Letters, 48 (2012), p. 919–921.
- [6] R. E. BLAHUT, *Fast algorithms for signal processing*, Cambridge University Press, Cambridge, UK, 2010.
- [7] S. BOUGUEZEL, M. O. AHMAD, AND M. N. S. SWAMY, *Low-complexity 8×8 transform for image compression*, Electronics Letters, 44 (2008), p. 1249–1250.
- [8] ———, *A novel transform for image compression*, in IEEE International Midwest Symposium on Circuits and Systems, 2010, p. 509–512.
- [9] R. N. BRACEWELL, *The Fourier transform and its applications*, McGraw-Hill, New York, NY, 2000.
- [10] W. L. BRIGGS AND V. E. HENSON, *The DFT: an owners' manual for the discrete Fourier transform*, vol. 45, SIAM, Philadelphia, PA, 1995.
- [11] E. O. BRIGHAM, *The fast Fourier transform and its applications*, Prentice-Hall, Inc., Englewood Cliffs, NJ, 1988.
- [12] V. BRITANAK, P. C. YIP, AND K. R. RAO, *Discrete cosine and sine transforms: general properties, fast algorithms and integer approximations*, Elsevier, Oxford, UK, 2010.
- [13] R. BUCHERT, S. SHAHRIER, AND P. BECKER, *Optimized discrete Fourier transform method and apparatus using prime factor algorithm*, 2004.
- [14] C. BURRUS AND P. ESCHENBACHER, *An in-place, in-order prime factor FFT algorithm*, IEEE Transactions on Acoustics, Speech, and Signal Processing, 29 (1981), pp. 806–817.
- [15] C. BURRUS, *DFT/FFT and convolution algorithms. Theory and implementation*, 1985.
- [16] S.-C. CHAN AND P. YIU, *An efficient multiplierless approximation of the fast Fourier transform using sum-of-powers-of-two (SOPOT) coefficients*, IEEE Signal Processing Letters, 9 (2002), pp. 322–325.
- [17] A. X. G. X. CHELLIAH, B. S. P. S. ROBINSON, M. SELLATHURAI, AND L. GOPALAKRISHNAN, *A power-efficient variable-length prime factor MDC FFT architecture for high-speed wireless communication applications*, AEU-International Journal of Electronics and Communications, 120 (2020), p. 153194.
- [18] R. CINTRA, *A note on the conversion of nonnegative integers to the canonical signed-digit representation*, arXiv preprint arXiv:2501.10908, (2025).
- [19] R. J. CINTRA, *An integer approximation method for discrete sinusoidal transforms*, Circuits, Systems, and Signal Processing, 30 (2011), p. 1481.
- [20] ———, *An approximation for the 32-point discrete Fourier transform*, arXiv, (2024).
- [21] R. J. CINTRA AND F. M. BAYER, *A DCT approximation for image compression*, IEEE Signal Processing Letters, 18 (2011), p. 579–582.
- [22] R. J. CINTRA, F. M. BAYER, AND C. TABLADA, *Low-complexity 8-point DCT approximations based on integer functions*, Signal Processing, 99 (2014), p. 201–214.
- [23] E. N. COMMITTEE ET AL., *Digital radio mondiale (DRM)—system specification*, ETSI ES, 201 (2009).
- [24] J. DAI AND H. YIN, *Design and realization of non-radix-2 FFT prime factor processor for 5G broadcasting in release 16*, in International Symposium on Computational Intelligence and Design, 2020, p. 406–409.
- [25] P. DUHAMEL AND M. VETTERLI, *Fast Fourier transforms: a tutorial review and a state of the art*, Signal Processing, 19 (1990), p. 259–299.
- [26] J. W. EATON, D. BATEMAN, AND S. HAUBERG, *GNU Octave Manual Version 3*, Network Theory Ltd., Oct. 2008.
- [27] M. EHRGOTT, *Multicriteria optimization*, vol. 491, Springer Science & Business Media, Heidelberg, BW, 2005.
- [28] B. EVERITT AND A. SKRONDAL, *The Cambridge dictionary of statistics*, vol. 106, Cambridge University Press Cambridge, New York, NY, 2002.
- [29] B. N. FLURY AND W. GAUTSCHI, *An algorithm for simultaneous orthogonal transformation of several positive definite symmetric matrices to nearly diagonal form*, SIAM Journal on Scientific and Statistical Computing, 7 (1986), p. 169–184.
- [30] M. FRIGO AND S. G. JOHNSON, *The fastest Fourier transform in the West*, tech. rep., Massachusetts Institute of Technology, 1997.
- [31] I. J. GOOD, *The interaction algorithm and practical Fourier analysis*, Journal of the Royal Statistical Society: Series B ), 20 (1958), p. 361–372.

- [32] R. I. HARTLEY, *Subexpression sharing in filters using canonic signed digit multipliers*, IEEE Transactions on Circuits and Systems II: Analog and Digital Signal Processing, 43 (1996), p. 677–688.
- [33] T. I. HAWHEEL, *A new square wave transform based on the DCT*, Signal Processing, 81 (2001), p. 2309–2319.
- [34] M. HEIDEMAN, C. BURRUS, AND H. JOHNSON, *Prime factor FFT algorithms for real-valued series*, in ICASSP'84. IEEE International Conference on Acoustics, Speech, and Signal Processing, vol. 9, IEEE, 1984, pp. 492–495.
- [35] M. T. HEIDEMAN AND C. S. BURRUS, *Multiplicative complexity, convolution, and the DFT*, Springer, New York, NY, 1988.
- [36] R. HEWLITT AND E. SWARTZLANTLER, *Canonical signed digit representation for FIR digital filters*, in IEEE Workshop on Signal Processing Systems, 2000, p. 416–426.
- [37] N. J. HIGHAM, *Computing the polar decomposition—with applications*, SIAM Journal on Scientific and Statistical Computing, 7 (1986), p. 1160–1174.
- [38] ———, *Computing real square roots of a real matrix*, Linear Algebra and its applications, 88 (1987), p. 405–430.
- [39] F. HOFMANN, C. HANSEN, AND W. SCHAFER, *Digital radio mondiale (DRM) digital sound broadcasting in the AM bands*, IEEE Transactions on Broadcasting, 49 (2003), p. 319–328.
- [40] R. A. HORN AND C. R. JOHNSON, *Matrix analysis*, Cambridge University Press, New York, NY, 2012.
- [41] S. G. JOHNSON AND M. FRIGO, *A modified split-radix FFT with fewer arithmetic operations*, IEEE Transactions on Signal Processing, 55 (2006), p. 111–119.
- [42] D.-S. KIM, S.-S. LEE, J.-Y. SONG, K.-Y. WANG, AND D.-J. CHUNG, *Design of a mixed prime factor FFT for portable digital radio mondiale receiver*, IEEE Transactions on Consumer Electronics, 54 (2008), p. 1590–1594.
- [43] ———, *Design of a mixed prime factor FFT for portable digital radio mondiale receiver*, IEEE Transactions on Consumer Electronics, 54 (2008), p. 1590–1594.
- [44] I. KITAMURA, S. KANAI, AND T. KISHINAMI, *Copyright protection of vector map using digital watermarking method based on discrete Fourier transform*, in IEEE International Geoscience and Remote Sensing Symposium, vol. 3, IEEE, 2001, p. 1191–1193.
- [45] K. KRISHNAGOWDA, R. KRAEMER, A. C. WOLF, AND E. R. BAMMIDI, *High-speed channel equalization scheme for 100 Gbps system*, in IEEE International Conference on Industrial Technology, 2018, p. 1430–1435.
- [46] S. KULASEKERA, A. MADANAYAKE, D. SUAREZ, R. J. CINTRA, AND F. M. BAYER, *Multi-beam receiver apertures using multiplierless 8-point approximate DFT*, in IEEE Radar Conference, 2015, p. 1244–1249.
- [47] S.-C. LAI, W.-H. JUANG, Y.-S. LEE, AND S.-F. LEI, *High-performance RDFT design for applications of digital radio mondiale*, in IEEE International Symposium on Circuits and Systems, 2013, p. 2601–2604.
- [48] D.-U. LEE, H. KIM, M. RAHIMI, D. ESTRIN, AND J. D. VILLASENOR, *Energy-efficient image compression for resource-constrained platforms*, IEEE Transactions on Image Processing, 18 (2009), p. 2100–2113.
- [49] S. LIN, N. LIU, M. NAZEMI, H. LI, C. DING, Y. WANG, AND M. PEDRAM, *FFT-based deep learning deployment in embedded systems*, in Design, Automation Test in Europe Conference Exhibition, 2018, p. 1045–1050.
- [50] N. LU, N. CHENG, N. ZHANG, X. SHEN, AND J. W. MARK, *Connected vehicles: Solutions and challenges*, IEEE Internet of Things Journal, 1 (2014), p. 289–299.
- [51] D.-K. LUN AND W.-C. SIU, *An analysis for the realization of an in-place and in-order prime factor algorithm*, IEEE Transactions on Signal Processing, 41 (1993), pp. 2362–2370.
- [52] A. MADANAYAKE, V. ARIYARATHNA, S. MADISHETTY, S. PULIPATI, R. J. CINTRA, D. COELHO, R. OLIVIERA, F. M. BAYER, L. BELOSTOTSKI, S. MANDAL, AND T. S. RAPPAPORT, *Towards a low-SWaP 1024-beam digital array: A 32-beam subsystem at 5.8 GHz*, IEEE Transactions on Antennas and Propagation, 68 (2019), p. 900–912.
- [53] A. MADANAYAKE, R. J. CINTRA, N. AKRAM, V. ARIYARATHNA, S. MANDAL, V. A. COUTINHO, F. M. BAYER, D. COELHO, AND T. S. RAPPAPORT, *Fast radix-32 approximate DFTs for 1024-beam digital RF beamforming*, IEEE Access, 8 (2020), p. 96613–96627.
- [54] K. MAHARATNA, E. GRASS, AND U. JAGDHOLD, *A 64-point Fourier transform chip for high-speed wireless LAN application using OFDM*, IEEE Journal of Solid-State Circuits, 39 (2004), p. 484–493.
- [55] H. MALVAR, A. HALLAPURO, M. KARCZEWICZ, AND L. KEROFSKY, *Low-complexity transform and quantization with 16-bit arithmetic for H. 26L*, in IEEE International Conference on Image Processing, vol. 2, 2002, p. II–II.
- [56] MATLAB, *version 8.1. (R2013a)*, The MathWorks Inc., Natick, Massachusetts, 2013.
- [57] P. A. MILDER, F. FRANCHETTI, J. C. HOE, AND M. PÜSCHEL, *Hardware implementation of the discrete Fourier transform with non-power-of-two problem size*, in IEEE International Conference on Acoustics, Speech and Signal Processing, 2010, p. 1546–1549.
- [58] S. H. MIRFARSHBAFAN, S. TANER, AND C. STUDER, *SMUL-FFT: a streaming multiplierless fast Fourier transform*, IEEE Transactions on Circuits and Systems II: Express Briefs, 68 (2021), pp. 1715–1719.
- [59] S. K. MITRA, *Digital signal processing: a computer-based approach*, McGraw-Hill Higher Education, 2001.
- [60] G. S. MOGHADAM AND A. A. B. SHIRAZI, *DOA estimation with co-prime arrays based on multiplicative beamforming*, in International Symposium on Telecommunications, 2018, p. 501–506.
- [61] D. G. MYERS, *Digital signal processing: efficient convolution and Fourier transform techniques*, Prentice-Hall, Inc., New York, NY, 1990.
- [62] H. J. NUSSBAUMER, *The fast Fourier transform*, in Fast Fourier Transform and Convolution Algorithms, Springer, Heidelberg, BW, 1981, p. 80–111.

[63] K. B. OLDHAM, J. MYLAND, AND J. SPANIER, *An atlas of functions: with equator, the atlas function calculator*, Springer Science & Business Media, New York, NY, 2010.

[64] A. V. OPPENHEIM, *Discrete-time signal processing*, Prentice-Hall, Upper Saddle River, NJ, 1999.

[65] L. PORTELLA, D. F. COELHO, F. M. BAYER, A. MADANAYAKE, AND R. J. CINTRA, *Radix-N algorithm for computing  $N^{2^n}$ -point DFT approximations*, IEEE Signal Processing Letters, 29 (2022), p. 1838–1842.

[66] U. S. POTLURI, A. MADANAYAKE, R. J. CINTRA, F. M. BAYER, AND N. RAJAPAKSHA, *Multiplier-free DCT approximations for RF multi-beam digital aperture-array space imaging and directional sensing*, Measurement Science and Technology, 23 (2012), p. 114003.

[67] S. QADEER, M. Z. A. KHAN, S. A. SATTAR, AND AHMED, *A radix-2 DIT FFT with reduced arithmetic complexity*, in IEEE International Conference on Advances in Computing, Communications and Informatics, 2014, p. 1892–1896.

[68] S. QIN, Y. D. ZHANG, AND M. G. AMIN, *Generalized coprime array configurations for direction-of-arrival estimation*, IEEE Transactions on Signal Processing, 63 (2015), p. 1377–1390.

[69] K. R. RAO AND P. C. YIP, *The transform and data compression handbook*, CRC press, Boca Raton, FL, 2018.

[70] G. A. SEBER, *A matrix handbook for statisticians*, John Wiley & Sons, Hoboken, NJ, 2008.

[71] J. SHI, G. HU, X. ZHANG, F. SUN, W. ZHENG, AND Y. XIAO, *Generalized co-prime MIMO radar for DOA estimation with enhanced degrees of freedom*, IEEE Sensors Journal, 18 (2017), p. 1203–1212.

[72] S. SONG, K. SONG, T. XU, W. ZHOU, H. LI, AND W. LIU, *The electronics design of real-time feedback control system in KTX*, IEEE Transactions on Nuclear Science, 68 (2021), p. 2066–2073.

[73] J. A. STANKOVIC, *Research directions for the Internet of Things*, IEEE Internet of Things Journal, 1 (2014), p. 3–9.

[74] J. Y. STEIN, *Digital signal processing: a computer science perspective*, John Wiley & Sons, Inc., New York, NY, 2000.

[75] D. M. SUÁREZ VILLAGRÁN, *Aproximações para a transformada discreta de Fourier e aplicações em deteção e estimação*, Master's thesis, Universidade Federal de Pernambuco, Recife, Brazil, 2015.

[76] D. M. SUÁREZ VILLAGRÁN, R. J. CINTRA, F. M. BAYER, A. SENGUPTA, S. KULASEKERA, AND A. MADANAYAKE, *Multi-beam RF aperture using multiplierless FFT approximation*, Electronics Letters, 50 (2014), p. 1788–1790.

[77] C. TABLADA, F. M. BAYER, AND R. J. CINTRA, *A class of DCT approximations based on the Feig–Winograd algorithm*, Signal Processing, 113 (2015), p. 38–51.

[78] L. H. THOMAS, *Using a computer to solve problems in physics*, Applications of Digital Computers, (1963), p. 44–45.

[79] P. P. VAIDYANATHAN AND P. PAL, *Sparse sensing with co-prime samplers and arrays*, IEEE Transactions on Signal Processing, 59 (2010), p. 573–586.

[80] M. D. VAN DE BURGWAL, P. T. WOLKOTTE, AND G. J. SMIT, *Non-power-of-two FFTs: Exploring the flexibility of the montium TP*, International Journal of Reconfigurable Computing, 2009 (2009).

[81] W. WANG, S. REN, AND Z. CHEN, *Unified coprime array with multi-period subarrays for direction-of-arrival estimation*, Digital Signal Processing, 74 (2018), p. 30–42.

[82] D. S. WATKINS, *Fundamentals of matrix computations*, vol. 64, John Wiley & Sons, New York, NY, 2004.

[83] K.-J. YANG, S.-H. TSAI, AND G. C. H. CHUANG, *MDC FFT/IFFT processor with variable length for MIMO-OFDM systems*, IEEE Transactions on Very Large Scale Integration (VLSI) Systems, 21 (2013), pp. 720–731.

[84] Z.-X. YANG, Y.-P. HU, C.-Y. PAN, AND L. YANG, *Design of a 3780-point IFFT processor for TDS-OFDM*, IEEE Transactions on Broadcasting, 48 (2002), p. 57–61.

[85] Z. ZHANG, X. WANG, K. LONG, A. V. VASILAKOS, AND L. HANZO, *Large-scale MIMO-based wireless backhaul in 5G networks*, IEEE Wireless Communications, 22 (2015), p. 58–66.